

# Lawrence Berkeley National Laboratory

## Recent Work

**Title**

NUCLEAR SCATTERING OF 300 MEV NEUTRONS

**Permalink**

<https://escholarship.org/uc/item/9z66w1r1>

**Author**

Ball, William Paul.

**Publication Date**

1952-08-01

UNIVERSITY OF CALIFORNIA - BERKELEY

UCRL- 1938

UIC

**TWO-WEEK LOAN COPY**

*This is a Library Circulating Copy  
which may be borrowed for two weeks.  
For a personal retention copy, call  
Tech. Info. Division, Ext. 5545*

**RADIATION LABORATORY**

## **DISCLAIMER**

This document was prepared as an account of work sponsored by the United States Government. While this document is believed to contain correct information, neither the United States Government nor any agency thereof, nor the Regents of the University of California, nor any of their employees, makes any warranty, express or implied, or assumes any legal responsibility for the accuracy, completeness, or usefulness of any information, apparatus, product, or process disclosed, or represents that its use would not infringe privately owned rights. Reference herein to any specific commercial product, process, or service by its trade name, trademark, manufacturer, or otherwise, does not necessarily constitute or imply its endorsement, recommendation, or favoring by the United States Government or any agency thereof, or the Regents of the University of California. The views and opinions of authors expressed herein do not necessarily state or reflect those of the United States Government or any agency thereof or the Regents of the University of California.

UCRL-1938  
Unclassified-Physics Distribution

UNIVERSITY OF CALIFORNIA

Radiation Laboratory

Contract No. W-7405-eng-48

NUCLEAR SCATTERING OF 300 MEV NEUTRONS

William Paul Ball

(Thesis)

August, 1952

Berkeley, California

TABLE OF CONTENTS

	Page
I INTRODUCTION	4
II ANALYSIS OF PROBLEM AND EXPERIMENT	8
A. Theory	8
B. General Features of Experiment	12
1. Elastic Scattering	12
2. Inelastic Scattering	13
III MEASUREMENT OF ELASTIC SCATTERING	15
A. Neutron Source and Spectrum	15
B. Apparatus and Electronics	17
1. Geometry	17
2. Beam Monitor	18
3. Neutron Detector	19
4. Electronics	20
C. Procedure	21
D. Validity	23
1. Background	23
2. Angular Resolution	24
3. Monitor Uniformity	24
4. Converter Effect	25
5. Variation of $d\sigma/d\Omega$ with Energy Cutoff Level in the Telescope	26
6. Check on Validity of the Method	26

	Page
E. Reduction of Data	28
1. Calculation of Cross Sections	28
2. Statistical Errors	35
F. Results	37
IV MEASUREMENT OF INELASTIC SCATTERING	38
A. Apparatus and Electronics	38
B. Procedure	40
C. Reduction of Data	41
1. Calculations of Cross Sections	41
2. Statistical Errors	43
D. Results	44
E. Attenuator in Proximity of Source Inelastic Arrangement	45
V CONCLUSIONS AND INTERPRETATIONS	46

## NUCLEAR SCATTERING OF 300 MEV NEUTRONS

William Paul Ball

### I INTRODUCTION

Experiments on the scattering of neutrons yield valuable results in the study of nuclear structure. Various nuclear models can be built around these results and generalized to provide the description of other nuclear properties. Below a few Mev the scattering is well described by a series of resonances.<sup>1</sup> At higher energies the neutron wave length becomes smaller than the nuclear diameter, and a region is approached, where the opaque physical optical model becomes valid. The scattering here is analagous to the scattering of light from an opaque sphere, and the total cross section is simply  $2\pi R^2$ .<sup>2,3</sup> Around 90 Mev the neutron wave length becomes still smaller, and the scattering mean free path for the neutron inside nuclear matter becomes comparable to the nuclear radius. This partial transparency gives rise to the transparent optical model of Fernbach, Serber, and Taylor.<sup>4</sup> Experimental results on the total cross sections at 84 Mev were obtained by Cook, McMillan, Peterson, and Sewell.<sup>5</sup> The Elastic and Inelastic components of the cross section at 84 Mev were obtained by Bratenahl, Fernbach, Hildebrand, Leith, and Moyer<sup>6</sup> and also by DeJuren and Knable<sup>7</sup> at 95 Mev. The above results were successfully described by the transparent optical model.

Total nuclear cross sections for 270 Mev neutrons were obtained by

DeJuren and Moyer<sup>8</sup> and by Fox, Leith, Wouters, and MacKenzie<sup>9</sup> at 280 Mev. DeJuren and Moyer also measured the total cross sections as a function of energy from 95 Mev up to 270 Mev for various nuclei. At these higher energies, the results deviated from those predicted by the transparent optical model. Above 100 Mev the cross sections dropped more rapidly with energy than predicted by the theory. It was suspected that the wave length of the neutron was becoming so small at these higher energies, that the neutron was beginning to see the nucleus as an assembly of nucleons rather than a homogeneous refractive medium. No entirely satisfactory theoretical fit to the data was obtained. Jastrow's Hard Core Model,<sup>10</sup> which assumes a strong rapidly rising repulsive potential at small separation of the nucleons, gave the most satisfactory fit, but even it was not entirely satisfactory. By measuring the elastic and inelastic cross sections individually, one could determine which of these components was responsible for the nuclear total cross section behavior at these energies.

In an attempt to shed some light on the above problem, Richardson, Leith, Moyer and the author collaborated to measure the nuclear elastic scattering cross sections for 340 Mev protons impinging on various substances.<sup>12,13</sup> Protons were chosen because of their uniformity in energy and their much higher detection efficiency than neutrons. Although these data were useful, the interpretation of the data at small angles, where the differential cross sections are the largest, was the least clear cut, due to the uncertainty in taking into account the contribution played by the coulomb forces compared to the nuclear forces. In addition,



if interpretive comparisons were to be made between these proton results and DeJuren's neutron results, assumptions would have to be made regarding the  $n-n$ ,  $n-p$ , and  $p-p$  forces.

A better comparison could be made in the above if neutron, rather than proton, elastic and inelastic cross sections were known. By comparing the neutron elastic and the proton elastic cross sections, one could also obtain information on how coulomb forces operate in nuclear regions.

Several difficulties are present in the determination of the above neutron cross sections. Some of the more prominent of the difficulties are: (a) The large spread in energy of the neutron beam causes ambiguities in the interpretation of the counts received. The cross sections are a function of energy. This results in a variable detection efficiency of neutrons with different energies, due to the variable loss of particles from nuclear collisions within the detector system. As a result, there is difficulty in assigning a cross section from the integrated data obtained over the entire energy spectrum. (b) The intensity of the cyclotron high energy neutron beam is low. (c) The detection efficiency of high energy neutron detectors is low.

The elastic and inelastic cross sections for the scattering of 300 Mev neutrons from representative nuclei have now been determined by the author. The first of the above difficulties, (a), was eliminated as follows: A method was devised whereby RATIOS of the counts in the scattered beam to the direct beam were obtained at all the measured angles rather than just the scattered counts alone. By definition,

elastic scattering contains only those scattered neutrons whose energy has not been changed, hence the spectrum of the elastically scattered neutrons is the same as the spectrum of the incident direct beam. By determining the above ratios, the effects of the variable detection efficiency due to the spread in the energy spectrum cancel out. Although these instrumental effects cancel, the cross sections obtained are not those of monoenergetic neutrons but represent cross sections averaged over the entire neutron energy spectrum. The results obtained were made more clear cut by reducing the extent of the neutron energy spread. This was accomplished by finding a more suitable neutron generator target than the beryllium target commonly employed for neutron beams. The second and third of the above difficulties, (b) and (c), were overcome by resorting to the use of a non-conventional "ring" scatterer rather than the usual "point" scatterer.

## II ANALYSIS OF PROBLEM AND EXPERIMENT

### A. THEORY

The cross sections for nuclear collisions with high energy neutrons are usually analyzed theoretically by the method of partial waves. A plane wave is expanded into a series of spherical harmonics<sup>14</sup> to represent the wave function of the incident neutron beam. The interaction of the incident wave with the scatterer nucleus results in phase shifts of some of the components. The wave function for the scattered neutron wave is obtained by subtracting the expression for the unperturbed incident plane wave from the solution for the case in which the scatterer nucleus is present. This may be represented asymptotically at large distances,  $r$ , from the scattering center and at an angle,  $\theta$ , from the incident beam by,

$$\Psi_{\text{scatt}} \approx \frac{e^{ikr}}{2ikr} \sum_{\ell=0}^{\infty} (2\ell+1) (e^{2i\delta_{\ell}} - 1) P_{\ell}(\cos \theta) \quad (1)$$

where the phase shift,  $\delta_{\ell}$ , is determined by matching the solution of the wave equation in the field free region to that within the boundaries of the scattering potential. If no absorption is present in the scattering nucleus,  $\delta_{\ell}$  is a real number and determines the phase shift between the  $\ell$ th partial wave of the diverging components of the wave function when the scatterer is present and the corresponding  $\ell$ th component of the unperturbed plane wave. When absorption is present,  $\delta_{\ell}$  is a complex number.

$$\delta_{\ell} = \alpha_{\ell} + i\beta_{\ell} \quad (2)$$

where  $\beta_l$  is the exponent determining the absorption of the  $l$ th partial wave.

The  $l$ th partial wave can be associated with particles in the beam which have an angular momentum of  $l\hbar$  with respect to the center of mass of the system, which for large nuclei is practically the center of the scattering nucleus. Since the wavelength of the incident particles at 300 Mev is appreciably smaller than the nuclear radius, it is sensible to speak of the particle colliding within the area represented by the cross section of the nucleus. If the impact parameter is  $b$ , the angular momentum is

$$pb = l\hbar, \text{ hence } l = pb/\hbar = b/\lambda = kb \quad (3)$$

The largest impact parameter at which nuclear forces can be felt is equal to  $R$ , the nuclear radius. Particles passing at larger distances should be unaffected, so that no components of the scattered beam should arise from  $l > kR$ . For 300 Mev neutrons impinging on lead, values of  $l = 1$  up to  $l = 39$  should be considered.

In the theory of the opaque nucleus, all particles which strike the nucleus are considered to be "absorbed", i.e. removed from the beam by inelastic processes. For this case  $\beta_l$  is infinite for  $0 \leq l \leq kR$ , and zero for  $l > kR$ ;  $\alpha_l$  is also zero for  $l > kR$ . For the absorbing sphere the scattered wave, Eq. (1), thus reduces to

$$\Psi_{\text{scatt}} \approx -\frac{e^{ikr}}{2ikr} \sum_{l=0}^{l=kR} (2l+1) P_l(\cos \theta) \quad (4)$$

These components of the scattered wave are equivalent to the corresponding outgoing components of the unperturbed plane wave shifted in

phase by 180°. This results in removing these outgoing components from the total wave field, which is the expected result for an absorbing sphere model of the nucleus. Putting these deficiencies or "holes" in the wave field gives the same intensity distribution of the diffraction pattern at large distances as would be obtained by adding corresponding in-phase excesses in amplitude to the field. The amplitudes in the two cases, however, differ in phase by 180 degrees. The above principle has its counterpart in physical optics, Babinet's principle.

The differential scattering cross section per unit solid angle is just the square of the amplitude of the scattered wave multiplied by  $r^2$ . It becomes,

$$\frac{d\sigma}{d\Omega}(\theta) = \frac{1}{4k^2} \left[ \sum_{l=0}^{l=kr} (2l+1) P_l(\cos \theta) \right]^2 \quad (5)$$

This distribution may be reduced with satisfactory approximation to the optical Fraunhofer diffraction pattern of plane light waves of wavelength  $\lambda = \frac{2\pi}{k}$  incident upon an opaque disc of radius  $R' = R + 1/k$ , which is usually given for small angles as,<sup>6</sup>

$$\frac{d\sigma}{d\Omega}(\theta) = k^2 (R')^4 \left[ \frac{J_1(2k R' \sin \frac{\theta}{2})}{2k R' \sin \frac{\theta}{2}} \right]^2 \quad (6)$$

where  $J_1$  is a first-order Bessel function.

If there is not complete absorption of those particles which strike the nucleus, the problem is one of diffraction of the incident wave by a sphere of material characterized by an index of refraction and an absorption coefficient. The index of refraction is due to the fact that

the magnitude of the propagation vector may change within the nucleus because of the nuclear potential well. The absorption coefficient arises from the interaction of the incident particle with individual nucleons in the nucleus, which is postulated to be the method of removing particles from the beam by inelastic processes. The absorption coefficient used by Fernbach, Serber, and Taylor<sup>4</sup> is just the numerical density of nucleons in the nucleus multiplied by the nucleon-nucleon scattering cross sections obtained from n-p and p-p scattering experiments and modified to allow for the suppression of small momentum transfers in the nucleus due to the Pauli exclusion principle. They obtain for a spherical scatterer with a non-reflecting surface

$$\Psi_{\text{scatt}} \approx \frac{e^{ikr}}{2ikr} \sum_{\ell=0}^{\ell+1/2 < kR} (2\ell+1) [e^{(-K+2ik_1)s_\ell} - 1] P_\ell(\cos \theta) \quad (7)$$

where  $k_1$  is the change in propagation constant,  $k$ , upon entering the nucleus;  $K$  is the absorption coefficient given by

$$K = \left( \frac{3}{4\pi R^3} \right) [Z \sigma_{np} + (A-Z) \sigma_{nn}] \quad (8)$$

and  $s_\ell$  is essentially the path length within the nucleus of the particle having angular momentum equal to  $\ell\hbar$ ,

$$s_\ell = \frac{[k^2 R^2 - (\ell + 1/2)^2]^{1/2}}{k} \quad (9)$$

The criterion for nonreflection is that the potential must not change appreciably within one wavelength. The cross sections  $\sigma_{np}$  and  $\sigma_{nn}$  in Eq. (8) are the effective n-p and n-n scattering cross sections for

collisions with nucleons in nuclei. The numerical values to be employed are obtained from known values of  $\sigma_{np}$  in free particle collisions, modified by effects of the Pauli principle. According to Goldberger,<sup>15</sup> this modification is,  $\sigma_{np} = 2/3 \sigma_{np}(\text{free})$ ;  $\sigma_{nn} = 1/4 \sigma_{np}$ .

## B. GENERAL FEATURES OF EXPERIMENT

### 1. Elastic Scattering

Neutrons emerging from the cyclotron are collimated both inside the shielding and on passing through the hole in the shielding, Figs. (1) and (2). On coming out of the 15 foot thick concrete shielding they pass through a thin sheet of polyethylene. Some of the neutrons knock protons out of the polyethylene and some of these resulting protons pass through a double coincidence crystal telescope beam monitor which counts them, Fig. (3). Most of the beam continues on undeviated. The collimator is 6 inches in diameter inside the shielding, and since the neutrons are coming from practically a "point" source in the cyclotron, the beam slowly diverges as it gets farther from the cyclotron. A 7 foot long steel billet, is centered in the beam and casts a neutron shadow behind it. Annular ring scatterers are slipped over a holder just beyond the billet. A triple coincidence stilbene crystal wide angle telescope, Figs. (4), (5), and (6); "sees" those scattered neutrons which happen to come at the correct angle to pass through it. The angle to the beam at which the telescope detector "sees" the scatterer, can be changed by moving the telescope nearer or farther from the scatterer along the axis of the beam. That part of the scattered neutron beam which leaves the

scatterer in the direction of the telescope passes through a 2 inch thick disc of copper to slow down or stop charged particles such as protons, so that they will not be able to pass through the telescope and make counts. After the beam is "filtered" by the above 2 inch copper proton stopper, it passes through a cylinder of polyethylene to convert some of these filtered neutrons into wanted protons. These protons then pass through the telescope and make triple coincidence counts. Wolfram absorbers can be inserted between the 2nd and 3rd crystals to stop converted protons whose energies are insufficient to pass through the absorber and make a triple coincidence count. By varying the wolfram thickness the level of the energy cutoff can be varied.

After the scattered beam is measured, the steel billet is removed and the detector telescope is left in the direct beam. A measurement in the direct beam is made. From the ratio of the scattered to the direct beam counts, absolute values can be calculated for the elastic differential scattering cross sections.

## 2. Inelastic Scattering

The ideal wide geometry would consist of a point detector located in the center of spherical shells of attenuator material. If this arrangement existed, as shells of attenuator material were put around the detector, the decrease in beam strength received by the detector would be due only to pure absorption of the neutrons in the attenuator. Those neutrons which originally would have passed into the detector but were scattered out of its path by the attenuator, would be compensated for by



others which would have missed the detector but were scattered into it. Furthermore, if the energy threshold of the detector could be set to reject those neutrons which had lost energy on being scattered, they would be included in the measured attenuation. It is this "poor" geometry attenuation which is referred to in this experiment as a measure of the "inelastic cross section". The elastic scattering cross section includes only those particles which have been scattered without losing energy. With the proper energy threshold in the detector, elastically scattered neutrons are recovered and count in the detector, while the inelastically scattered do not.

The wide geometry used in this experiment was not quite ideal, Figs. (7) and (8). It recovered only those particles which had been scattered between zero and  $32^\circ$ . It turns out, that at 300 Mev, the elastically scattered neutrons are overwhelmingly scattered in the neighborhood of the forward direction, so that the angular limitation is not serious.

The method used here is to put the inelastic scattering telescope setup in the direct 10-1/2 inch diameter beam. Counts are obtained with and without the attenuator in place. The measure of the attenuation of the beam furnishes information from which the inelastic scattering cross section can be calculated.

### III MEASUREMENT OF ELASTIC SCATTERING

#### A. NEUTRON ENERGY SPECTRUM

In scattering experiments it is desirable to have a beam of particles of as uniform an energy as possible. A clean separation can then be made between elastically and inelastically scattered particles on the basis of energy. Measurements previously made on the energy spectrum of the neutrons produced by the circulating proton beam inside the cyclotron tank impinging on an internal 2 inch beryllium target showed it to be very broad, about 100 Mev half width, with the peak energy around 270 Mev.<sup>16</sup> It was thought to be desirable to try to cut down this large spread in energy of the neutrons.

It was believed that deuterium, used as a target substance, might produce a more monoenergetic neutron beam than a corresponding beryllium target. This belief stemmed from the fact that although the loose neutron in deuterium has a greater binding energy, 2.20 Mev, than the loose neutron in beryllium, 1.6 Mev, the average kinetic energy and momentum of the deuterium neutron is considerably less than that in beryllium, since the deuterium neutron spends most of its time outside the nuclear potential well, where it has a high potential but low kinetic energy. Its average kinetic energy is of the order of the binding energy, 2 Mev. The average kinetic energy of the beryllium neutron, which spends most of its time inside the potential well is believed to be around 20 Mev. Because the incoming proton can meet neutrons in any of various momentum states, the energy of the emergent neutrons may be different for different

collisions depending upon the momentum state of the neutron in the target nucleus at the time of impact. This variability in momentum transfer will also cause a spreading out in the direction in which the neutrons come out. The neutrons emerging from beryllium nuclei with their larger internal momenta might thus have a larger spread in energy and direction than those coming out of deuterium. Since the beam used in this experiment comes out through the collimator in a relatively small solid angle in the forward direction, it is essentially the differential cross section in the forward direction  $d\sigma/d\Omega(0^\circ)$ , and not the total neutron production which determines the efficiency in producing our neutron beam. One might thus have a compound containing deuterium, which might produce a smaller total number of neutrons, but succeed in getting a larger number of them through the collimator than would, say, beryllium.

Because of its fair abundance of deuterium and convenience in handling etc., lithium deuteride was chosen as a target substance. It was successfully cast into a 1/2 inch thick block.<sup>17</sup> The neutron energy spectrum from it was determined by the author in collaboration with L. Neher, D. Dixon, R. E. Richardson, and M. Whitehead using a time of flight method of energy discrimination developed here by L. Neher. Because of the poor energy resolution of this method, only the area under the curves and not the details have any significance, Fig. (9). Making a comparison between the 1/2 inch thick Li D and the 3/16 inch thick beryllium, which because of density differences, expose the same number of nucleons to the circulating proton beam, it appears that the Li D target is getting a few more neutrons into the collimated beam than the corresponding Be.

A more accurate measurement and comparison of the neutron energy spectra than had hitherto been obtained was undertaken by the author in collaboration with W. Hess, J. Cladis and J. Wilcox, using a 35 channel magnetic spectrometer developed by J. Cladis, J. Hadley and W. Hess.<sup>16</sup> The energies of the various magnetic channels were calibrated by the current carrying stretched wire method.<sup>18</sup> The results obtained here were for a 2 inch beryllium target and 1/2 inch thick Li D, Fig. (10). Although the number of neutrons produced by the thinner Li D target was smaller than that produced by the thick Be target, the spectrum was considerably narrower, with a half width of about 42 Mev compared to the half width of 70 Mev for the thick Be target. This fact alone made the 1/2 Li D for this particular experiment, far superior to the customary 2 inch Be. An additional encouragement toward this end was the fact that the accidental coincidence rate prevented the utilization of the maximum beam, so that even the 1/2 inch Li D furnished more neutrons than could be utilized. The 1/2 inch Li D was used throughout this experiment. J. DePangher, of this laboratory, is making a study of the efficiency and energy spectrum from thicker Li D targets using high pressure cloud chamber techniques.

## B. APPARATUS AND ELECTRONICS

### 1. Geometry

Conventional methods, such as narrow telescope counters "looking" at small scattering targets were tried. They were quickly discarded when it was found, that in spite of intensive efforts to reduce the

background counting rate, the scattered neutron counts were so few as to be insufficiently above the background. It was decided to use a non-conventional "line" source of scatterer in place of the usual "point" source. The type of geometry decided on is shown in Figs. (1) and (2).

The tapered solid iron billet in the figure is lined up with its axis along the axis of the beam. It is 7 feet long and is 6 inches in diameter at the end away from the cyclotron. It is situated outside the 15 foot thick concrete shielding of the cyclotron and is located 60 feet from the neutron source target inside the cyclotron tank. It is a frustrum of a right circular cone, which, if extended, would have its apex at the neutron source target. The purpose of the billet is to cast a neutron shadow, so that the neutron detectors can be located inside the shadow. The scattering targets are annular rings, which are slipped over a holder and are located just beyond the end of the shaft. The annular rings vary from one to six inches long and all have an inside diameter of 6 inches and an outside diameter of 8 inches. The beam is approximately 8-1/2 inches in diameter at the target location, and hence completely bathes the target in a uniform beam of neutrons, Fig. (11).

## 2. Beam Monitor

The beam monitor is a bridge type double coincidence stilbene crystal telescope which "looks" at protons knocked out of a thin sheet of polyethylene located in the beam, Figs. (1) and (3). The output is amplified by a 5 mc band width linear amplifier and fed into a scalar. The unit was designed and built by Dwight Dixon and Leland Neher of this laboratory.

### 3. Neutron Detector

The neutron detector is a triple coincidence wide angle stilbene crystal telescope, Figs. (4), (5) and (6). It consists of three 1P21 photomultiplier tubes each looking at light pulses from its respective trans-stilbene crystal. The front crystal is  $7/8$  inch square by  $1/8$  inch thick. The middle crystal is 2 inches square by  $1/4$  inch thick. The third or rear crystal is 5 inches in diameter and  $1/2$  inch thick. It was grown at this laboratory by C. André, J. Carothers, and J. Steller. The neutrons entering the detector telescope system must first pass through a two inch thick plate of copper in order to slow down or stop the charged particle impurity such as protons, etc. in the beam. The neutrons then pass through a  $1-1/2$  inch diameter by  $1-1/2$  inch long cylinder of polyethylene. Part of them are converted to protons in the forward direction by the n-p reaction. These converted protons then pass through the three stilbene scintillators. Various thicknesses of wolfram proton energy reducers are placed between the second and third crystals to stop converted protons below a selected energy, Figs. (4) and (7). Wolfram was chosen for these absorbers because of its high mass density,  $19.3 \text{ g/cm}^3$  and accordingly its high electron density. This property gives it a high linear efficiency in slowing down charged particles. As a result, it occupies a minimum of space between the 2nd and 3rd crystals and allows them to be closely spaced. This gives the telescope a maximum angular acceptance with a given size rear crystal. For the above wide angle telescope with a 5 inch rear crystal and a 4 inch spacing between the 2nd and 3rd crystals, a maximum theoretical angle of

acceptance of  $\tan^{-1} 2.5/4 = 32^\circ$  was obtainable.

The telescope assembly is supported by an I beam rail, which runs parallel to the axis of, but below the neutron beam, Fig. (1). The angular setting of the telescope is changed by moving it along the beam axis. When the telescope is set near the scatterer, it accepts only neutrons which have been scattered through a wide angle, whereas if it is placed far from the scatterer, it accepts only neutrons which have been scattered through a small angle. The practical angular range with the limited length of rail used in the experiment ran from 2 degrees to 20 degrees.

#### 4. Electronics

The coincidence circuit used in this experiment is a modified Rossi type of triple coincidence circuit using a crystal diode as a diode clamp in the plate circuit and a crystal diode signal expander circuit in the output. It was designed and constructed here by R. Madey, B. Ragent, and P. Nikonenko and is similar to one devised by Garwin.<sup>19</sup> Light pulses from each of the stilbene scintillators were viewed by 1P21 photomultipliers. The electrical pulses from the three 1P21 photomultipliers were clipped to  $2 \times 10^{-8}$  second duration by means of shorted coaxial lines. These pulses were then amplified by 100 mc wide band amplifiers and fed into the above coincidence unit, Fig. (12). The coincidence circuit has a resolving time of  $2 \times 10^{-8}$  seconds with these pulses. The outputs from the coincidence units are amplified by standard 5 mc band width linear amplifiers and fed into scalers.

Two of the above coincidence units were used in this experiment. Into one of them was inserted a delay line corresponding to  $6.3 \times 10^{-8}$  second delay in one of its three inputs. The signal in this branch of the input arrives one r.f. cycle of the cyclotron later than the other two signals. If the three signals were from the same proton and had started about the same time, the delay of one of them would prevent a coincidence from being registered. A certain number of coincidences are accidental coincidences due to overlapping in time of separate events. These "accidentals" are essentially as likely to register when one of the inputs to the coincidence unit is delayed by one r.f. cycle of the cyclotron. The unit with the delay thereby measures the accidental rate. A subtraction of these accidentals from the total counts of the undelayed unit then gives a measure of the true counts. The method was checked by observing the change in accidental rate with beam strength. The variation of accidental counts/monitor with change in beam strength was essentially quadratic as had been expected.

### C. PROCEDURE

A cathetometer is positioned beyond the location of the apparatus and is centered in the 8-1/2 inch diameter beam by photographing the beam with chest x-ray films. Rings with cross wires are mounted on the billet support in place of the billet. The support is then lined up with the beam by sighting through the cathetometer and lining the cross wires of the support rings with the cross hairs of the cathetometer. The rail along which the neutron detector telescope is moved is similarly lined up with the cathetometer by means of cross wires. The telescope



is then set on the rail at the  $2^{\circ}$  position. The neutron monitor telescope is mounted in position. After the electronics have been checked for plateaus, Fig. (23), etc., a run is made with the detector telescope in the direct beam, and a value for the triples minus accidentals/monitor counts is obtained. This is repeated for the various telescope energy cutoffs which are to be used in the scattered beam. The steel billet is then carefully placed in a calibrated position on its support. The scatterer target holder is mounted on the far end of the billet and a scatterer ring target is placed in position. A run is made with the neutron telescope now in the scattered beam, and another triples minus accidentals/monitor counts is obtained. The scatterer target is removed and a third triples minus accidentals/monitor counts is obtained. These last three sets of values are repeated for settings of the telescope position along the rail corresponding to various scattering angles and for the several scattering targets. It is not necessary to repeat the direct beam measurements for the various rail settings, since it is known that the beam changes in intensity as the inverse square of the distance from the Li D neutron generator target inside the cyclotron. This latter point was checked experimentally. Having obtained the direct beam value at the one position, the direct beam values at all the other positions can be calculated knowing their respective distances from the Li D target. When the above measurements had been made, the billet and its support were removed and the neutron detector telescope system with its paraphenalia were mounted on a short rail, which in turn was mounted on a rotary table. The triples minus accidentals/monitor values were obtained

at various settings straddling the range of scattered neutron angles determined. A curve for the angular efficiency of the telescope system was thus obtained. This was repeated for the various telescope energy cutoffs used in the scattered beam. The relative change in efficiency with angle was found not to be significantly different for the different energy cutoffs, hence a master curve for all of them was adopted. The angular efficiency did not change appreciably from one set of runs to another, so it was not found necessary to continually repeat its determination, once it had been determined.

#### D. VALIDITY

##### 1. Background

First crude attempts at using the annular ring setup were met with high background counting rates. The background rates were comparable to the scattered beam counting rates. The background rate was reduced by a factor of a hundred by, (a) building a 7 foot long tapered lead collimator inside the igloo near the cyclotron, Fig. (1); (b) placing three one inch thick brass annular rings of increasing inside diameter, coaxially in series with one another in front of the copper proton stopper in front of the neutron detector telescope, Figs. (4) and (6); and (c) carefully aligning the system with the beam. The background counting rate subsequently became one to ten percent of the scattered beam, depending on the scatterer and the scattering angle. It was measured for every experimental point obtained in the scattered beam and was accounted for.

The effect of that part of the iron billet support, which sits in the neutron beam when the billet is in place, is to contribute slightly to the background counting rate. When the direct beam measurement was made with the billet removed, but its support still in place, the magnitude of the effect compared to that of the direct beam was believed to be small. Measurements made to check the effect showed it to be undetectable.

## 2. Angular Resolution

The limits of angular resolution with the annular ring setup turned out to be a constant fraction of the scattering angle. In this case it was approximately  $\theta/3$ . For an angle of, say  $9^\circ$ , it was  $\pm 3^\circ$  while at a setting of  $3^\circ$ , it was  $\pm 1^\circ$ . This turned out to be one of the good features of this system. At small angles where the differential cross sections are large, the spread in angular acceptance is small and vice versa. This tended to equalize the counting rates over the entire angular range used.

## 3. Monitor Uniformity

In the elastic experiment, in order to keep the accidental coincidence rate low, the strength of the beam is reduced by a factor of 50 in going from the scattered beam to the direct beam. It is imperative that the monitor's response be linear over this range. This was checked over a range exceeding that used in the experiment as follows: The neutron telescope was set at a given angle in the scattered beam using the 3 inch lead scatterer. The beam strength was varied in steps

through a range straddling all the values used in the experiment.

Throughout the entire range, the ratio of triples-acid/monitor remained constant, indicating a constant efficiency for the monitor over this range. If it did unknowingly vary, it did so in exactly the same way as the telescope efficiency, and its effect was harmless.

#### 4. Converter Effect

To be sure that we were counting protons converted from neutrons, we observed the counting rates with the polyethylene converter in place and with it removed. The counting rate increased by a factor greater than three when the converter was inserted in place. This was considered a favorable ratio, since some of the neutrons are converted to protons on passing through the first crystal, and a number of others are converted elastically inside the 2 inch copper proton stopper, Figs. (4) to (6). If these latter are converted near the exit side of the copper, they will lose little energy before emerging from it and hence will behave in a similar manner to those actually converted inside the polyethylene converter. The copper proton stopper is 5-1/2 inches in diameter, hence a question might arise about the possibility that an appreciable number of converted protons coming from this disc might come from wide angles, thereby deteriorating the angular resolution expected from the telescope system. To check this point, a complete angular distribution was made for neutrons scattered from the lead target without the converter in place, to see if it would be appreciably different from that obtained with the converted in place, Fig. (16). It is evident from the figure,

that there is no appreciable difference in the distributions obtained both with and without the converter in place. This indicates that the converted protons in the copper disc, are overwhelmingly those converted in the forward direction with the neutrons. Their effect, then, is essentially the same as those converted in the polyethylene, hence they have no appreciable deleterious effect on the angular resolution.

##### 5. Variation of $d\sigma/d\Omega$ With Energy Cutoff Level

There might have been a possibility that the cross sections obtained using different thicknesses of wolfram absorber between the 2nd and 3rd crystals in the telescope, that is, different rejection energy levels could have given different results in the cross sections. This would be particularly true if there were a substantial number of neutrons which lost only a small amount of energy on being scattered either inelastically or quasi-elastically.<sup>18,20</sup> To check this, cross sections were obtained using a range of wolfram absorbers corresponding to rejection energy cutoffs from 187 Mev to 258 Mev, Fig. (13). It is evident from the figure that the cross sections obtained over a wide range of decelerators remained essentially constant, showing that if the particles lose energy in being scattered, they either lose a very large amount of energy or very little.

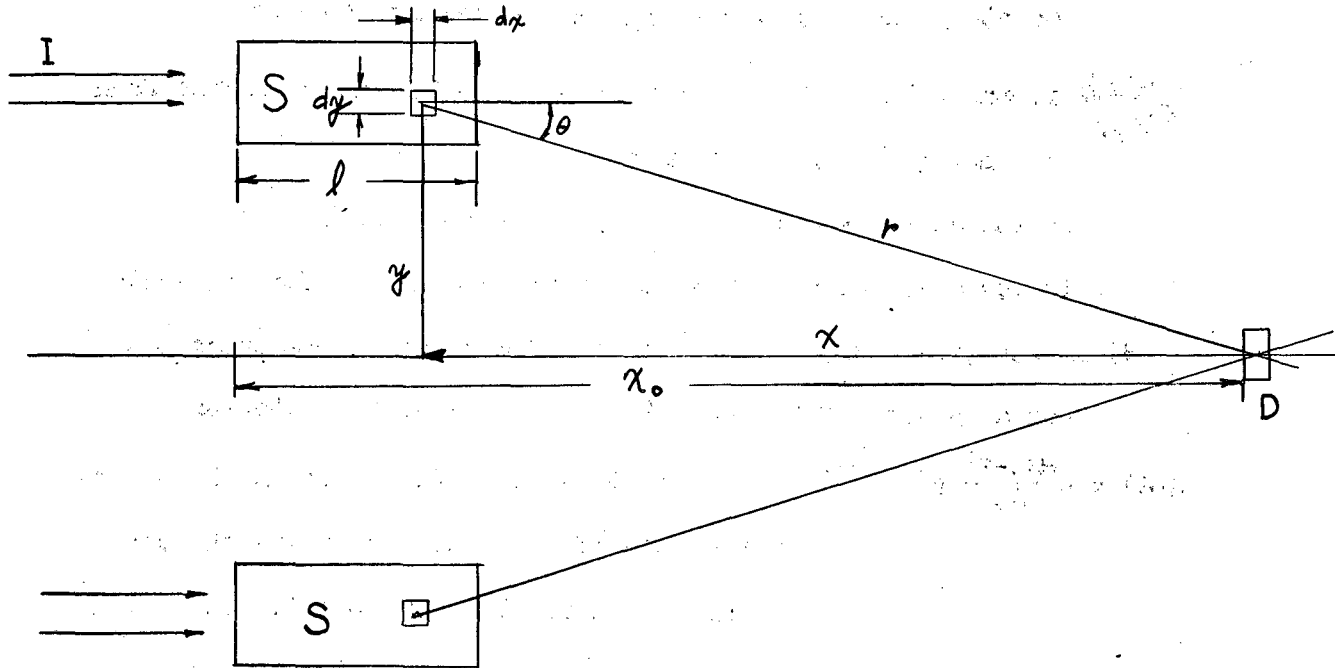
##### 6. Check on Validity of the Method

In order to feel confident that no major hidden factors had been overlooked, it was decided to repeat the measurement of the angular distribution of elastically scattered neutrons at lower energy, i.e., 90 Mev

which had previously been determined by other methods.<sup>6</sup> As a representative sample, the angular distribution of elastically scattered 90 Mev neutrons from copper was chosen. The one inch thick copper ring was used for the scatterer. The 90 Mev neutrons were obtained from 190 Mev deuterons impinging on a 1/2 inch thick beryllium target just as has been done in the above reference. The results are shown in Fig. (14). It is evident from the figure that the fit of our data with those previously determined was extremely good. This placed a strong measure of confidence on the method and apparatus. Our confidence was even further extended when data taken months apart from each other checked with each other satisfactorily.

E REDUCTION OF DATA

1. Calculation of Cross Sections



The number of counts detected by the neutron detector, D, which are scattered from the differential volume element  $2 \pi y dx dy$  in the scatterer, S, at an angle  $\theta$  can be written,

$$dC = I \frac{\rho N_0}{A} 2 \pi y dx dy \frac{d\sigma}{d\Omega}(\theta_{x,y}) \frac{a \cos \theta_{x,y}}{r^2(x,y)} \eta(\theta_{xy}) G(\theta_{x,y}) \quad (10)$$

where,

I is the incident neutron flux density on the target

$\frac{\rho N_0}{A}$  is the numerical density of the scattering nuclei

$\rho$  is the mass density in  $\text{g/cm}^3$  of the scattering material

A is the atomic weight of the scattering material

No is Avogadro's number

$\frac{d\sigma}{d\Omega}(\theta)$  is the differential elastic scattering cross section for the scatterer nucleus at an angle  $\theta$  to the incident beam

$\frac{a \cos \theta}{r^2(x,y)}$  is the solid angle of neutrons received by the detector from a point (x,y) in the source

a is the effective aperture of the telescope for  $\theta = 0$

r is the distance from the scattering element to the telescope

$\eta(\theta)$  is the efficiency of the detector for detecting neutrons coming from an angle  $\theta$  with respect to the axis of the detector

$G(\theta) = e^{-\frac{(x_0-x)}{\lambda t}} e^{-\Delta(\theta)/\lambda}$  is the attenuation factor of the beam along the path of the neutrons inside the scatterer. It involves two parts: (a) Total cross section removal of the beam before it gets to the point of scattering, resulting in a lower effective beam at that point, and, (b) Inelastic cross section attenuation of the scattered beam for the balance of the neutron path,  $\Delta$ , in the scatterer. The inelastic cross section is used here, because, as a fair approximation, the scattered neutron sees a wide angle geometry for the balance of its path such as is described on page (13).



$l$  is the depth of the scatterer

$\lambda_t = \frac{A}{\rho N_0 \sigma_t}$  is the mean free path for the neutrons in the scatterer

$\sigma_t$  is the total cross section for the removal of neutrons from the beam by a target nucleus

$\lambda_i = \frac{A}{\rho N_0 \sigma_i}$  is the mean free path for inelastic collisions for the neutrons in the scatterer

$\sigma_i$  is the inelastic cross section

Integrating the above differential counting rate over the entire scatterer we write the following integral,

$$C = \frac{K}{A} \frac{\rho N_0 2\pi a}{A} \int_{x_0-l}^{x_0} dx \int_{y_1}^{y_2} dy \left\{ y \cos \theta_{xy} \frac{d\sigma}{d\Omega}(\theta_{xy}) \frac{\eta(\theta_{xy})}{r_{xy}^2} G(\theta_{xy}) \right\} \quad (11)$$

Since the functions in the integrand are well-behaved and single valued, it will be assumed that a mean value angle can be found, such that the integrand at this angle multiplied by the range will give the same integrated value as the above integral. Having assumed this, we will treat several parts of the integrand as constant and bring them outside the integral sign:

$$C = \frac{K \frac{d\sigma}{d\Omega}(\bar{\theta}) \eta(\bar{\theta}) \cos \bar{\theta} G(\bar{\theta})}{r^2} \int_{x_0-l}^{x_0} dx \int_{y_1}^{y_2} y dy$$

$$= I_a \left[ \frac{\rho N_0}{A} \pi (y_2^2 - y_1^2) l \right] \frac{\frac{d\sigma}{d\Omega}(\bar{\theta}) \eta(\bar{\theta}) \cos \bar{\theta} G(\bar{\theta})}{r^2} \quad (12)$$

The quantity inside the square bracket is just  $N$ , the total number of scatterer nuclei.

The number of counts received by the detector in the direct beam, when the detector is tilted to the direct beam by the same angle as the scattering angle and located at the same scattering position is,

$$C_0 = I_0 a \cos \bar{\theta} \eta(\bar{\theta}) \quad (13)$$

Taking the ratio of (12) and (13) we obtain,

$$\frac{C}{C_0} = \frac{I \cos \bar{\theta} N \eta(\bar{\theta}) \frac{d\sigma}{d\Omega}(\bar{\theta}) G(\bar{\theta})}{I_0 \cos \bar{\theta} \eta(\bar{\theta}) r^2} \quad (14)$$

Assuming the detector and monitor had the same efficiency in both the scattered and the direct beam measurements, we can express the number of counts as,

$$\frac{C}{M} = E I; \quad \frac{C_0}{M_0} = E I_0 \quad (15)$$

Where E is the efficiency of the detector.

Substituting the I's from (15) in (14) and cancelling out the E's, we get for the differential elastic scattering cross section,

$$\frac{d\sigma}{d\Omega}(\bar{\theta}) = \frac{\frac{C}{M} r^2}{\frac{C_0}{M_0} N G(\bar{\theta})} \quad (16)$$

C and C<sub>0</sub> are the true counts after the background and accidental counts have been subtracted. M and M<sub>0</sub> are the corresponding monitor counts. Instead of turning the telescope at the scattering angle  $\theta$  and using it at every scattering position in the direct beam to obtain the various C<sub>0</sub>'s, we can substitute the simpler experimental expedient described on page 23. If we do this, equation (16) finally becomes,

$$\frac{d\sigma(\bar{\theta})}{d\Omega} = \frac{c r^2}{C_0 \frac{\eta(\theta)}{\eta(0)} \frac{R^2(\theta')}{R^2(\theta)} N G(\bar{\theta})} \quad (17)$$

$$\text{where } C = \frac{T_1 - A_1}{M_1} - \frac{T_2 - A_2}{M_2}$$

$T_1$  = total triple coincidence counts with scatterer in beam

$A_1$  = accidental triple coincidence counts with scatterer in beam

$M_1$  = corresponding monitor counts

$T_2$  = total triple coincidence counts with scatterer removed

$A_2$  = accidental triple coincidence counts with scatterer removed

$M_2$  = corresponding monitor counts

$$C_0 = \frac{T_0 - A_0}{M_0}$$

$T_0$  = total triple coincidence counts with telescope at some rail position in the direct beam, (usually the  $2^\circ$  position), and pointed parallel to the beam at an angle  $0^\circ$  to the beam

$A_0$  = corresponding accidental triple coincidence counts

$M_0$  = corresponding monitor counts

$\bar{r}^2$  = distance squared from the effective scattering center of the scatterer to the center of the front crystal in the telescope

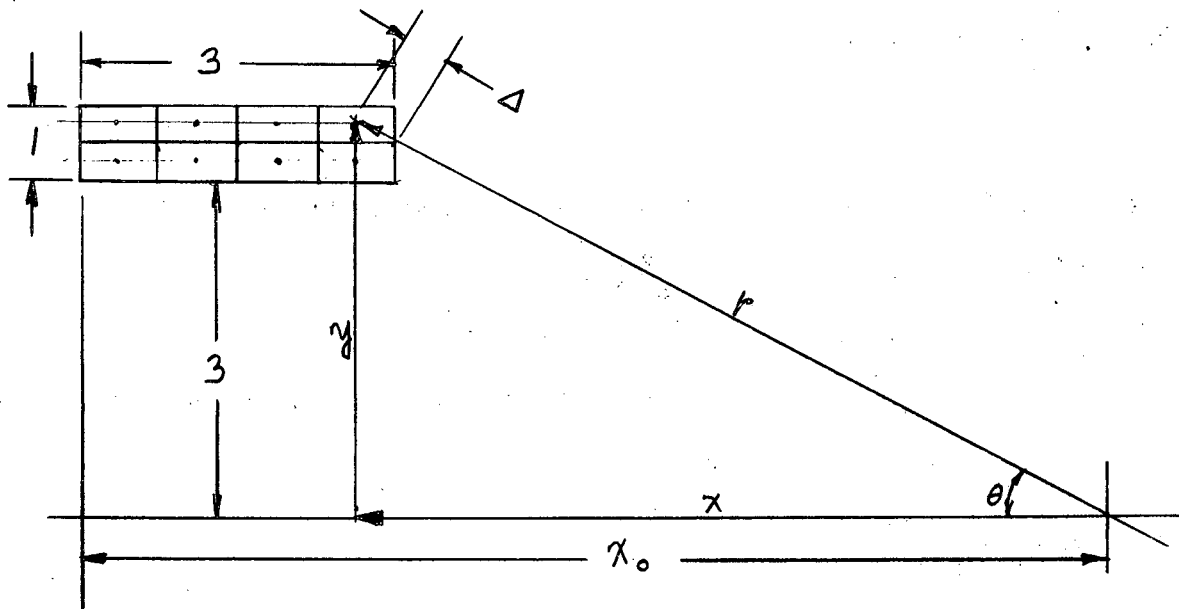
$$G(\bar{\theta}) = e^{-\frac{(x_0 - x)}{\lambda l}} - \frac{\Delta(\bar{\theta})}{\lambda l} \quad (\text{see page 29})$$

$\frac{\eta(\bar{\theta})}{\eta(0)}$  = relative angular efficiency of telescope system at angle  $\bar{\theta}^\circ$  to that at  $0^\circ$  (obtained from angular efficiency curve)

$R(\theta')$  = distance from LiD target inside cyclotron to the position of the telescope during the direct beam measurement

$R(\theta)$  = distance from LiD target inside cyclotron to the rail position of the scattering angle  $\theta$

The mean values used in Equation (17) are calculated by approximate methods.



A weighting factor can be assigned to a point (x,y) for its efficiency in getting neutron counts into the telescope,

$$\xi(xy) = \frac{\eta(\theta_{xy}) y^2}{r_{xy}^2} e^{-\left[ (x_0 - x) + 2/3 \Delta(\theta_{xy}) \right] / \lambda_t} \frac{d\sigma}{d\Omega}(\theta_{xy}) \quad (18)$$

$$\theta = \tan^{-1} \frac{y}{x}$$

$\eta(\theta)$  is obtained from the experimentally determined angular efficiency curve for the neutron telescope system.

$e^{-\left[ (x_0 - x) + 2/3 \Delta(\theta_{xy}) \right] / \lambda_t} = G(\theta_{xy})$ , where the average ratio of inelastic mean free path to total mean free path for the elements used is assumed for all of them. This is  $\lambda_i \approx 3/2 \lambda_t$ . The  $\lambda_i$ 's were determined in the inelastic part of this experiment.

The theoretical mean values can be expressed as,

$$\bar{\theta} = \frac{\int_{y_1}^{y_2} \int_{x_1(y)}^{x_2(y)} \xi(x,y) \theta(x,y) dx dy}{\int_{y_1}^{y_2} \int_{x_1(y)}^{x_2(y)} \xi(x,y) dx dy} \quad (19)$$

$$\bar{r}^2 = \frac{\int_{y_1}^{y_2} \int_{x_1(y)}^{x_2(y)} \xi(x,y) r^2(x,y) dx dy}{\int_{y_1}^{y_2} \int_{x_1(y)}^{x_2(y)} \xi(x,y) dx dy} \quad (20)$$

In actual calculations, the integrals are approximated by summations,

$$\bar{\theta} = \frac{\sum_i \xi(x_i y_i) \theta(x_i y_i)}{\sum_i \xi(x_i y_i)} \quad (21)$$

$$\bar{r}^2 = \frac{\sum_i \xi(x_i y_i) r^2(x_i y_i)}{\sum_i \xi(x_i y_i)} \quad (22)$$

The cross section of the scatterer annular ring is divided up into rectangles. In the case of the 3 inch thick scatterer, there were taken 8 rectangles 1/2 inch x 3/4 inch each. In the case of the one inch thick scatterers there were four 1/2 inch x 1/2 inch squares. In all cases, the effect of each rectangle was assumed to be due to its geometrical center and the summation of the effects was summed over these geometrical centers. The relatively small magnitudes of the corrections indicated that finer subdivisions were not necessary. The mean values  $\bar{\theta}$  and  $\bar{r}^2$  are obtained by the method of successive approximations. The geometrical center is taken for the zeroth approximation. Assuming all the scattering is taking place from the center, a calculation is made, Equation (17) and a  $\frac{d\sigma}{d\Omega}(\theta_0)$  is obtained. Substituting this  $\frac{d\sigma}{d\Omega}$  into equation (18), we obtain  $\xi_1$ 's(x,y). Substituting  $\xi_1$ 's in equations (21) and (22), first approximations for the various  $\bar{\theta}_1$ 's and  $\bar{r}_1^2$ 's are determined. These in turn can be substituted back in

equation (17) and a new  $\frac{d\sigma}{dn}(\bar{\theta}_1)$  determined. In principle, this process can be repeated indefinitely, each time getting a better approximation to the differential cross section. The rapidity of convergence was not established in this experiment, when it was found that the first order correction in most cases was less than the statistical errors. The values quoted in this experiment have only been corrected to the first order.

## 2. Errors

To determine the statistical errors of the cross sections, the individual errors of the various components going into the cross section formula were compounded according to the usual formula,

$$\delta F^2(x_1 x_2 x_3 \dots) = \left(\frac{\partial F}{\partial x_1}\right)^2 \delta x_1^2 + \left(\frac{\partial F}{\partial x_2}\right)^2 \delta x_2^2 + \left(\frac{\partial F}{\partial x_3}\right)^2 \delta x_3^2 + \dots \quad (23)$$

For this experiment,

$$F = \frac{d\sigma}{dn} = \frac{C F^2}{C_0 \frac{\eta(\theta)}{\eta(0)} \frac{R^2(\theta')}{R^2(\theta)} N G(\theta)} \quad (17)$$

The statistical errors of the  $\eta$ 's can be neglected for simplification. The individual  $\eta$  points were determined to a statistical accuracy of around two percent, and the graph of the many points should be even more statistically significant.

The only other factors which are of a statistical counting nature are the C's. In the case of

$$C \approx \frac{T_1}{M_1}$$

$$C_0 \approx \frac{T_0}{M_0},$$

for simplification, we neglect the background errors, since in every instance they were determined to an absolute accuracy considerably better than were the scattered counts. The accidental rate errors,  $A_1$  and  $A_2$  and  $A_0$  will be neglected for the same reason. Making the above approximations, equation (17) is differentiated with respect to  $T_1$ ,  $M_1$ ,  $T_0$ , and  $M_0$  and put in a convenient form for computation. The resulting formula becomes

$$\delta F = \frac{T^2 R^2(\theta) M_0 \eta(0)}{N R^2(\theta') (T_0 - A_0) M_1 \eta(\theta)} \left[ T_1 + A_1 + (T_1 - A_1)^2 \left\{ \frac{T_0 + A_0}{(T_0 - A_0)^2} + \frac{1}{M_1} + \frac{1}{M_0} + \frac{0.256}{\left( \frac{\eta(\theta)}{\eta(0)} \right)^2} \right\} \right]^{\frac{1}{2}} \quad (24)$$

The scalars were always set to a scale of 64, hence the above formula has been adjusted to take care of the fact that the T's, A's, and M's put into this formula are really 1/64th of the total actual counts. The  $\delta F$ 's are the statistical errors indicated on the angular distribution of elastic scattering graphs.

Errors of a non-statistical nature can also arise from the approximations made in obtaining the correction values. These are not expected to be excessive.

## F RESULTS

The elastic scattering results are shown in Figs. (16) to (21) and Table I. The theoretical Fraunhofer diffraction patterns, indicated by the solid lines in the figures, were calculated from equation (6). The radii used in the theoretical calculations were taken to be those of an opaque sphere, whose maximum cross sectional area was equal to the inelastic cross section determined in this experiment.

The results from lead would seem to fit the diffraction pattern quite well if the theoretical pattern were smeared by the experimental angular resolution. The fit to a diffraction pattern gets progressively worse as one goes to lighter elements. For carbon the deviation is large.

The differential elastic cross sections were multiplied by their solid angles and integrated graphically over the measured range of angles. The results are shown in Table II. When the integrated elastic results are added to the inelastic cross sections, determined in the second part of this experiment, the sums found are all in agreement with the corresponding total cross sections of DeJuren and Moyer,<sup>8</sup> within statistical errors.



#### IV MEASUREMENT OF INELASTIC SCATTERING

##### A APPARATUS AND ELECTRONICS

The experimental arrangement for the inelastic measurements is seen in Figures (7) and (8). A wide angle geometry was used (see Section II-B-2 for general method). The electronics, the beam monitor, and the neutron detector telescope were the same as those used in the elastic part of the experiment with the exception that the detector had been modified as described below.

In the elastic experiment, the angular resolution was an important factor. For this reason, the smallest of the three crystals was put in the front position, with the next larger and the largest crystals following along the beam in that order. The "optics" of this system could be considered as having the scattered beam particles cross over the axis in the middle of the first crystal. This allowed the use of a small diameter polyethylene converter, 1-1/2 inches diameter, which would still convert efficiently out to an angle of  $18^\circ$  and yet could not seriously increase the spread in the angular resolution. This system, however, limited the angular acceptance of the telescope to  $27^\circ$ . In the inelastic experiment, a wide angle geometry (so-called "poor geometry") was used. With this system all the angles were collected at once to give an integrated inelastic cross section. There was no need for good angular resolution there, hence a large diameter polyethylene converter could be used. The order of the first two crystals could then be reversed, with the smallest crystal placed in the middle position between the first and third crystals. With this type of "optics",

the particles cross over in the center of the middle crystal, and the angular acceptance of the telescope system is increased to 32 degrees. The telescope, along with the 1 inch thick polyethylene converter, is placed behind a series of six large one inch thick neutron beam attenuator discs.

As a check on the reliability of the experimental arrangement, it was decided to repeat the determination of the inelastic cross section on copper at 90 Mev, which had previously been done by Bratenahl, et al.<sup>6</sup>; and by DeJuren and Knable.<sup>7</sup> An uncorrected value of  $\sigma_i = 0.910$  barns was found for the inelastic cross section. Assuming the total cross section of Cook, McMillan, Peterson, and Sewell,<sup>5</sup> we get for the ratio  $\frac{\sigma_i}{\sigma_t} = 0.41$ , which is in agreement within statistical error to the values found by Bratenahl et al. and of DeJuren and Knable of  $\frac{\sigma_i}{\sigma_t} = 0.39$ . If the usual fine correction for the angular efficiency of the telescope had been determined at this energy, the agreement should have been even closer.

B PROCEDURE

The neutron detector telescope is lined up with and in the center of the neutron beam by using x-ray film photographs of the beam just as the cathetometer had been in the elastic experiment. Two one inch thick copper attenuators are placed in front of the telescope to slow down or stop the charged particle contamination of the beam. A run is made, and the counts/monitor determined. Four more one inch thick attenuator discs are placed in front of the telescope and the run repeated. A new counts/monitor is determined. This was carried out for carbon, aluminum, copper, and lead attenuators. The telescope arrangement with the two one inch thick copper attenuators was then mounted upon a rotary table and an angular efficiency curve was determined. From these results, combined with a correction factor explained below, the inelastic cross sections were calculated.

C REDUCTION OF DATA

1. Calculation of Cross Sections

Since the beam is attenuated exponentially in passing through the attenuator, we can write,

$$N = N_0 e^{-\frac{l}{\lambda_i}} = N_0 e^{-n \sigma_i l} \quad (25)$$

where

$N_0$  is the number of neutrons entering an attenuator

$N$  is the number of neutrons left after they have passed through a thickness of attenuator,  $l$

$l$  is the thickness of the attenuator

$\lambda_i$  is the mean free path for inelastic scattering of the neutrons in the attenuator

$n$  is the number of nuclei per  $\text{cm}^3$  in the attenuator material

$\sigma_i$  is the inelastic cross section per nucleus

Taking the logarithm of both sides of (25),

$$\ln \frac{N}{N_0} = -n \sigma_i l$$

or,

$$\sigma_i = \frac{1}{n l} \ln \frac{N_0}{N} \quad (26)$$

Assuming an overall constant detection efficiency,  $E$ , for the detector and monitor system, both with the attenuator in place and with it removed,

$$\frac{T_0 - A_0}{M_0} = E N_0 \quad (27)$$

$$\frac{T_i - A_i}{M_i} = E N \quad (28)$$

where

$T_0$  is the total number of triple coincidences counted with the attenuator out

$A_0$  is the number of corresponding accidental coincidences

$M_0$  is the number of corresponding monitor counts

$T_1$  is the total number of triple coincidence counts with the attenuator in

$A_1$  is the number of corresponding accidental coincidences

$M_1$  is the number of corresponding monitor counts

Substituting (27) and (28) in (26) and cancelling the E's,

$$\sigma_i = \frac{1}{n \cdot l} \ln \frac{\frac{T_0 - A_0}{M_0}}{\frac{T_1 - A_1}{M_1}} \quad (29)$$

The efficiency of the neutron detector decreases with increasing angle, hence the number of neutrons elastically scattered in the attenuator and subsequently detected are fewer than would be detected if the detection efficiency were the same at all angles as it is at zero degrees. This effect gives too large an apparent attenuation. The resulting inelastic cross section is too large. To get the corrected inelastic cross section, the effect of this excess attenuation has to be subtracted from equation (29). It is given by

$$\delta = 2\pi \int_0^{\theta_{\max}} \left[ 1 - \eta(\theta) \right] \frac{d\sigma(\theta)}{d\Omega} \sin \theta \, d\theta \quad (30)$$

This correction term is obtained graphically from the elastic scattering data and the inelastic angular efficiency curve. These corrections only

amounted to about one percent for lead and two percent for carbon. Combining equations (29) and (30), the corrected inelastic cross section becomes,

$$\sigma_i = \frac{1}{n\ell} \ln \frac{\frac{T_o - A_o}{M_o}}{\frac{T_i - A_i}{M_i}} - 2\pi \int_0^{\theta_{\max}} [1 - \eta(\theta)] \frac{d\sigma}{d\Omega}(\theta) \sin\theta d\theta \quad (31)$$

where

$\eta(\theta)$  is the relative efficiency of the inelastic telescope system at an angle  $\theta^\circ$  to that at the angle  $0^\circ$  (obtained from the inelastic telescope angular efficiency curve)

$\frac{d\sigma}{d\Omega}(\theta)$  is the differential elastic scattering cross section obtained from the elastic scattering experiment

$d\theta$  is the differential angle in radians

The above development has neglected the effect of multiple scattering of neutrons in the attenuator. Approximate calculations showed this effect to be less than three percent in all cases. Since this is less than the statistical error, no attempt was made to correct for it.

## 2. Statistical Errors

Again referring to equation (23), applying it to equation (31), and neglecting the error in the correction second term and the error in the accidentals, we obtain,

$$\delta \sigma_i = \pm \frac{1}{n\ell} \sqrt{\frac{1}{T_o} + \frac{1}{M_o} + \frac{1}{T_i} + \frac{1}{M_i}} \quad (32)$$

These errors are statistical standard deviations.

D RESULTS

The inelastic results are shown in Table II. When added to the integrated elastic cross sections obtained in the first part of this experiment, the resulting total cross sections obtained are found to be in agreement with the total cross sections obtained at these energies by DeJuren and Moyer.

E ATTENUATOR IN PROXIMITY OF SOURCE WIDE ANGLE INELASTIC ARRANGEMENT

The author, in collaboration with J. DeJuren, made an early attempt to determine the inelastic cross section for 300 Mev neutrons on copper using a non-conventional wide geometry setup, Fig. (15). Instead of the conventional neutron detector with wide angular acceptance and the broad attenuator placed against it, the broad attenuator was placed inside the cyclotron tank near the neutron generating target at a great distance from the detector. This interchanged the role of the detector and the neutron source in their ability to allow widely scattered neutrons to be gathered and detected. Because of space limitations, the arrangement only allowed the collection of elastically scattered neutrons up to about ten degrees. This limited the method to attenuators with high atomic number to insure the collection of a substantial fraction of the elastically scattered neutrons. This inconvenient and limited method was abandoned, when it was found practicable to construct crystal coincidence detectors with wide angular acceptance. Nevertheless, it is interesting to note, that the values obtained in separate measurements using this method for copper turned out to be 0.73, 0.75, and 0.72 barns respectively. These values compare favorably with the value of 0.75 barns found later by the wide angle telescope system.



## V CONCLUSIONS AND INTERPRETATIONS

When DeJuren and Moyer obtained their unexpected drop in cross sections with energy above 100 Mev, further progress depended on determining whether it was the elastic part of the cross section or the inelastic part that was responsible for the drop. The results of this experiment, when compared with lower energy results, show that the drop in total cross section is primarily due to the elastic component of the total cross section.

In Table III the results of this experiment at 300 Mev are compared with those obtained by DeJuren and Knable<sup>7</sup> at 95 Mev. It is seen in the table that the inelastic cross section has changed very little between the two energies. The elastic cross section, on the other hand, has changed by more than a factor of two in all cases.

A simple physical picture of what may be happening at these higher energies is that the wave packet, representing the incoming neutron, is becoming so highly concentrated in a small region, that is beginning to feel the effects of the individual nucleons. This effect is more pronounced as one goes to higher energies and as one goes to elements of lower nucleon density. With respect to neutrons of these energies, the lighter nuclei act simply like swarms of essentially independent nucleons, and thus fail to demonstrate effects such as diffraction which depend upon the nucleus behaving as a unit.

S. Fernbach<sup>21</sup> made calculations to fit the transparent model to the total cross section results of DeJuren and Moyer at 270 Mev, as he had done for the 90 Mev data. For the best fit to the data, he obtained a value

of  $k_1 = 0$ . This was a very striking result, in that it implied an index of refraction equal to unity, or an effective nuclear potential equal to zero, for the neutron passing through the nucleus.

Jastrow<sup>11</sup> calculated the index of refraction in terms of the forward scattering amplitudes for the n-n and n-p interactions, using both his own hard core model of the nucleon<sup>10</sup> along with the model proposed by Christian and Hart<sup>22</sup> for the n-p interaction and Christian and Noyes<sup>23</sup> for the n-n (actually p-p) interaction and the experimental p-p data of Chamberlain, Segré and Wiegand.<sup>24,25</sup> The hard core model, too predicted a rapid decrease in the index of refraction and  $k_1$  going to zero. It was even small at 160 Mev. The fit to DeJuren's data was good in all but the intermediate energy region.

Fernbach took  $k_1 = 0$  and calculated an absorption coefficient,  $K$ , which would best fit the experimental data. He obtained  $K = 2.3 \times 10^{12} \text{ cm}^{-1}$ . From this he calculated the variation of the inelastic cross section with atomic number to be expected on the basis of the above values of  $k_1$  and  $K$ , Fig. (22). The experimental values obtained from this experiment are plotted in the same figure for comparison. As seen in the figure, his predictions agree very well with the experimental data obtained in this experiment.

Table IV shows a comparison between the 300 Mev neutron differential elastic scattering cross sections of this experiment with the corresponding 340 Mev proton cross sections of Richardson, Ball, Leith, and Moyer.<sup>12,13</sup> The 340 Mev proton carbon cross sections at small angles appear to be in error. The curve in the above reference rises unexpectedly at small angles, and the data do not check the neutron values. Aluminum, copper, and lead

show increasing coulomb effect in that order as expected. It has become appreciable for copper and lead at  $6^\circ$ , more so than was expected when the proton experiment was performed. A careful theoretical analysis will be necessary before more quantitative conclusions can be drawn about the effect of the coulomb forces.

ACKNOWLEDGEMENTS

The author wishes to express his thanks to Prof. Burton J. Moyer for suggesting the problem and for his invaluable guidance and assistance throughout the work; to Prof. Ernest O. Lawrence for his inspiration and interest in this work; to the 184- inch cyclotron crew for their continued help; to Dr. Robert E. Richardson for his assistance in the construction of the apparatus; to Mrs. Vivian Koblick for her assistance in carrying out the computations; and last but not least to the various members of Prof. Moyer's group who assisted in the collection of the data.

This work was carried out under the auspices of the Atomic Energy Commission.

REFERENCES

1. Lecture Series in Nuclear Physics MDDG 1175
2. E. Amaldi, D. Bocciarelli, B. Cacciapuoti, and G. Trabachi, *Nuovo Cimento* 3, 203 (1946)
3. R. Sherr, *Phys. Rev.* 68, 240 (1945)
4. S. Fernbach, R. Serber, and T. Taylor, *Phys. Rev.* 75, 1352 (1949)
5. L. Cook, E. McMillan, J. Peterson, and D. Sewell, *Phys. Rev.* 75, 7 (1949)
6. A. Bratenahl, R. H. Hildebrand, C. E. Leith, and B. J. Moyer, *Phys. Rev.* 75, 7 (1949)
- X 7. J. DeJuren and N. Knable, *Phys. Rev.* 77, 606 (1950)
- X 8. J. DeJuren and B. J. Moyer, *Phys. Rev.* 81, 919 (1951)
9. R. Fox, C. Leith, L. Wouters, and K. MacKenzie, *Phys. Rev.* 80, 23 (1950)
10. R. Jastrow, *Phys. Rev.* 81, 636 (1951)
11. R. Jastrow, *Phys. Rev.* 82, 261 (1951)
12. R. E. Richardson, W. P. Ball, C. E. Leith, and B. J. Moyer, *Phys. Rev.* 83, 859 (1951)
13. R. E. Richardson, W. P. Ball, C. E. Leith, and B. J. Moyer, *Phys. Rev.* 86, 29 (1952)
14. J. W. Strutt, *Proc. London Math. Soc.* (1) IV, 253 (1873)
15. M. L. Goldberger, *Phys. Rev.* 74, 1268 (1948)
16. J. B. Cladis, J. Hadley, and W. N. Hess, *Phys. Rev.* 86, 110 (1952)
17. R. McKisson, UCRL-992

18. J. B. Gladis, Phys. Rev. 87, 425 (1952)
19. R. L. Garwin, Rev. Sci. Instr. 21, 569 (1950)
20. P. Wolff, Phys. Rev. 87, 434 (1952)
21. S. Fernbach, Thesis, UCRL-1382
22. R. Christian and E. Hart, Phys. Rev. 77, 441 (1950)
23. R. Christian and H. P. Noyes, Phys. Rev. 79, 85 (1950)
24. O. Chamberlain, E. Segre, and C. Wiegand, Phys. Rev. 81, 284 (1951)
25. O. Chamberlain and C. Wiegand, Phys. Rev. 79, 81 (1950)

TABLE I  
DIFFERENTIAL ELASTIC SCATTERING CROSS SECTIONS

3 in. C Scatt.			3 in. Al Scatt.			1 in. Cu Scatt.		
Angle $\bar{\theta}$	$\frac{d\sigma}{d\Omega}(\bar{\theta})$	$\delta$	Angle $\bar{\theta}$	$\frac{d\sigma}{d\Omega}(\bar{\theta})$	$\delta$	Angle $\bar{\theta}$	$\frac{d\sigma}{d\Omega}(\bar{\theta})$	$\delta$
2.02	1.202	± 0.118	2.02	4.820	± 0.412	2.02	14.25	± 0.93
3.24	0.928	± 0.069	3.23	4.124	± 0.544	3.23	9.98	± 0.58
4.23	0.831	± 0.064	4.22	3.090	± 0.262	4.22	8.32	± 0.33
5.24	0.688	± 0.053	6.23	1.597	± 0.131	5.20	5.38	± 0.37
6.25	0.595	± 0.052	9.11	0.786	± 0.063	6.18	3.54	± 0.22
7.22	0.469	± 0.034	11.95	0.282	± 0.024	7.15	2.43	± 0.16
9.16	0.323	± 0.026	13.85	0.194	± 0.016	8.11	1.309	± 0.091
11.10	0.203	± 0.019	15.93	0.108	± 0.013	9.08	0.813	± 0.042
12.05	0.167	± 0.014	18.00	0.093	± 0.013	10.05	0.584	± 0.050
13.95	0.125	± 0.011				11.00	0.395	± 0.031
15.80	0.083	± 0.010				11.95	0.274	± 0.022
17.65	0.052	± 0.007				13.00	0.238	± 0.021
						14.05	0.206	± 0.021
						15.08	0.176	± 0.017
						18.15	0.135	± 0.015

1 in. Pb Scatt.

Angle $\bar{\theta}$ (deg)	$\frac{d\sigma}{d\Omega}(\bar{\theta})$	$\delta$
2.02	79.47	± 3.20
4.12	23.65	± 1.27
5.10	10.11	± 0.73
6.09	5.21	± 0.33
7.12	2.33	± 0.17
8.15	1.485	± 0.104
9.13	1.080	± 0.056
10.11	0.796	± 0.076
11.08	0.715	± 0.048
12.05	0.513	± 0.042
13.05	0.389	± 0.038
14.05	0.395	± 0.045
15.10	0.324	± 0.034
18.25	0.202	± 0.023

3 in. Cu Scatt.

Angle $\bar{\theta}$ (deg)	$\frac{d\sigma}{d\Omega}(\bar{\theta})$	$\delta$
2.02	14.59	± 0.68
3.24	11.15	± 0.50
4.23	8.08	± 0.38
5.22	5.45	± 0.28
6.20	3.69	± 0.19
7.15	2.38	± 0.12
8.09	1.316	± 0.070
9.04	1.013	± 0.052
9.98	0.616	± 0.036
10.91	0.475	± 0.024
11.85	0.294	± 0.018
12.90	0.249	± 0.014
13.95	0.214	± 0.013
16.10	0.171	± 0.024
18.25	0.135	± 0.013

TABLE I  
DIFFERENTIAL ELASTIC SCATTERING CROSS SECTIONS

3 in. Pb Scatt.

Angle $\theta$ (deg)	Polyethylene Converter in		Polyethylene Converter Removed
	$\frac{d\sigma}{d\Omega}(\theta)$	$\delta$	$\frac{d\sigma}{d\Omega}(\theta)$
2.02	75.55	$\pm 3.69$	78.48
3.25	44.13	$\pm 1.95$	51.6
4.24	24.62	$\pm 1.12$	
5.18	11.69	$\pm 0.60$	
6.11	5.24	$\pm 0.33$	6.40
7.11	2.62	$\pm 0.14$	
8.12	1.37	$\pm 0.078$	
9.10	1.22	$\pm 0.070$	
10.08	0.799	$\pm 0.051$	
11.02	0.777	$\pm 0.045$	
11.95	0.557	$\pm 0.066$	
13.85	0.404	$\pm 0.025$	
15.70	0.305	$\pm 0.025$	
17.55	0.194	$\pm 0.021$	0.280

TABLE II  
INTEGRATED ELASTIC, INELASTIC AND TOTAL CROSS SECTIONS

	Integrated differential elastic cross section (barns) $\sigma_e$	Inelastic cross section $\sigma_i$ (barns)		$\sigma_{e+i}$	$\sigma_{\text{total}}$	$\sigma_{\text{total}}$
				(barns)	DeJuren and Moyer <sup>6</sup> (barns)	$\frac{i \text{ this expt.}}{t}$ DeJuren and Moyer
C	0.079	0.203 $\pm 0.033$		0.282	0.288	0.70
Al	0.187	0.390 $\pm 0.023$		0.577	0.555	0.70
Cu	0.410	0.755 $\pm 0.033$		1.17	1.15	0.66
Pb	1.339	1.72 $\pm 0.08$		3.06	2.84	0.61



TABLE III

VARIATION OF COMPONENT NEUTRON CROSS SECTIONS WITH ENERGY

Element	$\sigma_{el}^*$	$\sigma_{el}^{**}$	$\frac{\sigma_{el300}}{\sigma_{el195}}$	$\sigma_{inel}^*$	$\sigma_{inel}^{**}$	$\frac{\sigma_{inel300}}{\sigma_{inel195}}$
	300 Mev	95 Mev		300 Mev	95 Mev	
C	0.079	0.274	0.288	0.203	0.222	0.914
Al	0.187	0.577	0.324	0.390	0.418	0.933
Cu	0.410	1.223	0.335	0.755	0.782	0.965
Pb	1.339	2.71	0.494	1.72	1.75	0.983

\* This Experiment

\*\* DeJuren and Knable<sup>7</sup>

TABLE IV

COMPARISON OF 300 MEV NEUTRON AND 340 MEV PROTON DIFFERENTIAL

ELASTIC SCATTERING CROSS SECTIONS AT SMALL ANGLES

Element	$\frac{d\sigma}{d\Omega}(5^\circ)^*$ Neut.	$\frac{d\sigma}{d\Omega}(5^\circ)^{**}$ Prot.	$\frac{d\sigma}{d\Omega}(6^\circ)^*$ Neut.	$\frac{d\sigma}{d\Omega}(6^\circ)^{**}$ Prot.
C	0.725	1.866	0.600	0.905
Al	2.40	2.61	1.80	2.137
Cu	6.00	9.51	3.88	5.248
Pb	13.5	33.8	4.70	12.71

\* This Experiment

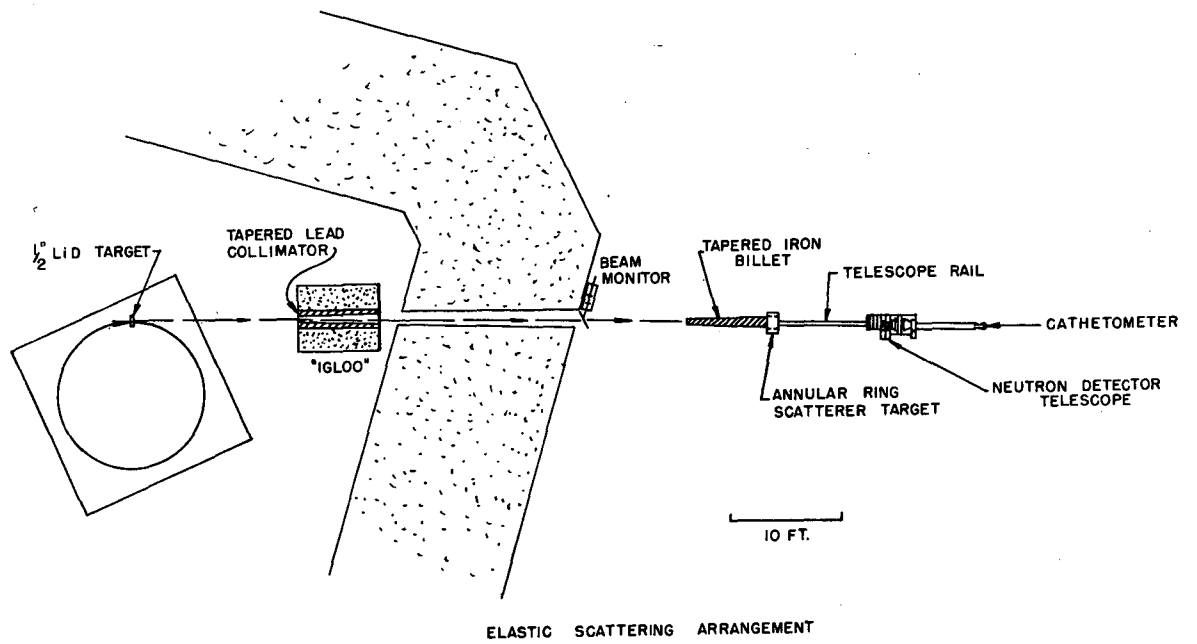
\*\* Richardson, Ball, Leith, and Moyer<sup>12,13</sup>

FIGURE CAPTIONS

- Fig. 1 Diagram of Experimental Arrangement
- Fig. 2 Photograph of Experimental Arrangement
- Fig. 3 Double Coincidence Crystal Telescope Beam Monitor
- Fig. 4 Diagram of Neutron Detector Telescope
- Fig. 5 Side View Photograph of Neutron Detector Telescope
- Fig. 6 Quarter View Photograph of Neutron Detector Telescope
- Fig. 7 Diagram of Inelastic Setup
- Fig. 8 Photograph of Inelastic Setup
- Fig. 9 Graph of Neutron Energy Spectra by Time of Flight Method
- Fig. 10 Graph of Neutron Energy Spectra by Magnet Spectrometer Method
- Fig. 11 X-Ray Photograph of Beam Pattern with Elastic Scattering Experimental Setup in the Beam
- Fig. 12 Photograph of Coincidence Unit
- Fig. 13  $\frac{d\sigma}{d\Omega}$  vs. Rejection Energy Level in the Neutron Detector Telescope
- Fig. 14  $\frac{d\sigma}{d\Omega}$  vs.  $\theta$  for 90 Mev Neutrons on Copper
- Fig. 15 Diagram of Attenuator in Proximity of Source Wide Angle Inelastic Arrangement
- Fig. 16  $\frac{d\sigma}{d\Omega}(\theta)$  vs.  $\theta$  for Lead (3 in. Thick) with Polyethylene n,p Converter in and with it Removed
- Fig. 17  $\frac{d\sigma}{d\Omega}(\theta)$  vs.  $\theta$  for Carbon (3 in. thick scatterer)
- Fig. 18  $\frac{d\sigma}{d\Omega}(\theta)$  vs.  $\theta$  for Aluminum (3 in. thick scatterer)
- Fig. 19  $\frac{d\sigma}{d\Omega}(\theta)$  vs.  $\theta$  for Copper (1 in. thick scatterer)
- Fig. 20  $\frac{d\sigma}{d\Omega}(\theta)$  vs.  $\theta$  for Lead (1 in. thick scatterer)
- Fig. 21  $\frac{d\sigma}{d\Omega}(\theta)$  vs.  $\theta$  for Copper (3 in. thick scatterer)

Fig. 22 Graph of fit of data to Transparent Model Theory

Fig. 23 Coincidence Unit Voltage Plateau



MU 4082

Fig. 1

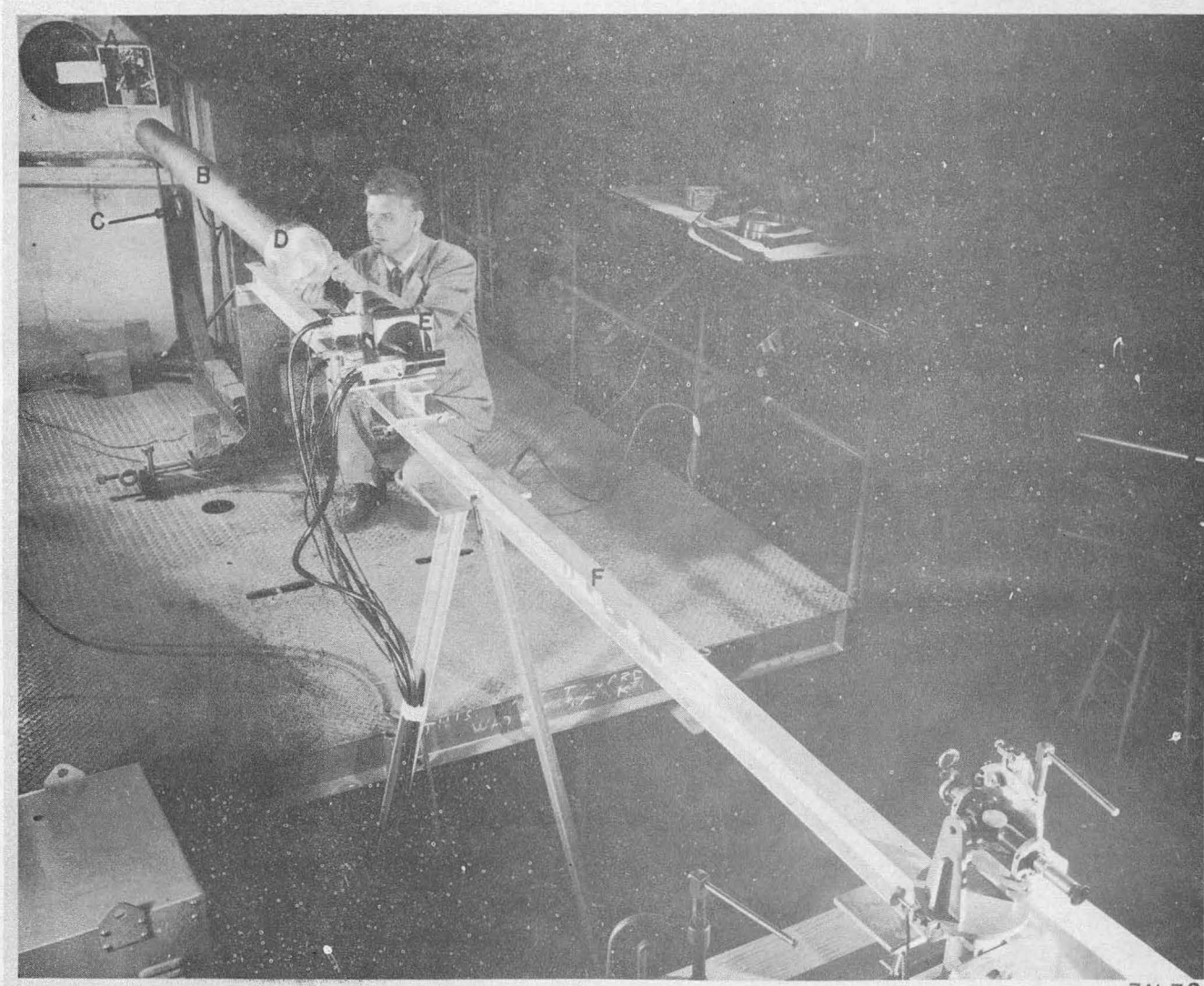
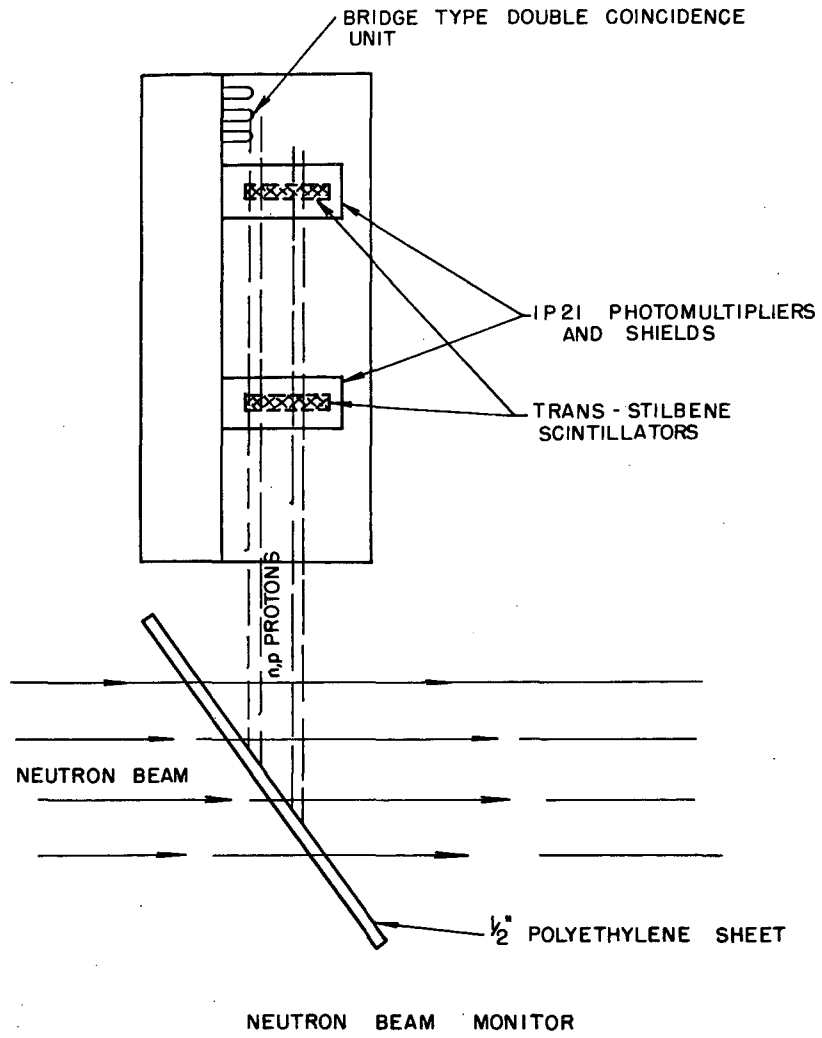
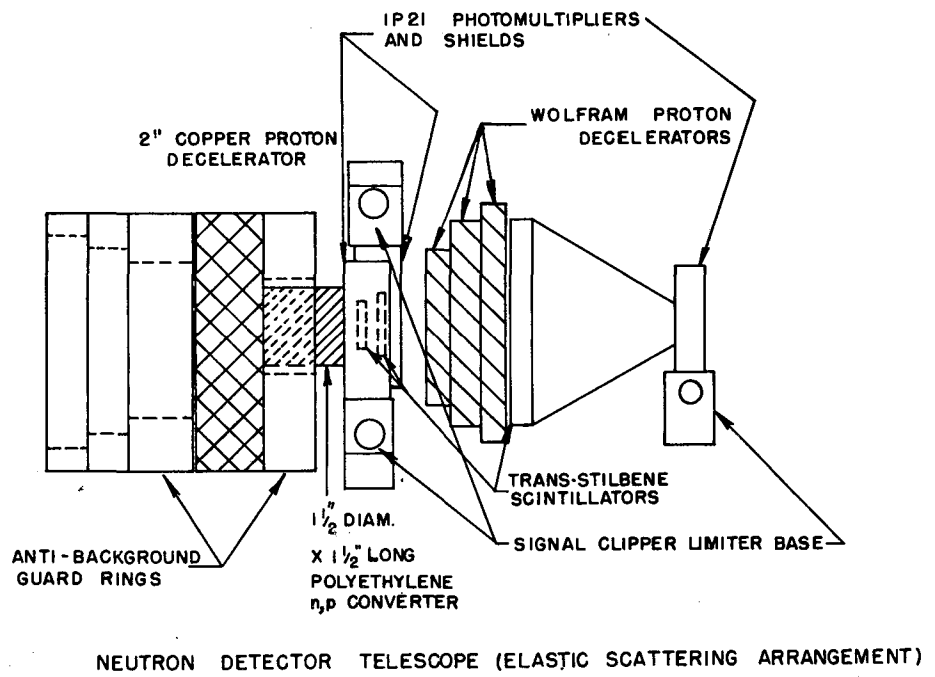


Fig. 2



MU4113

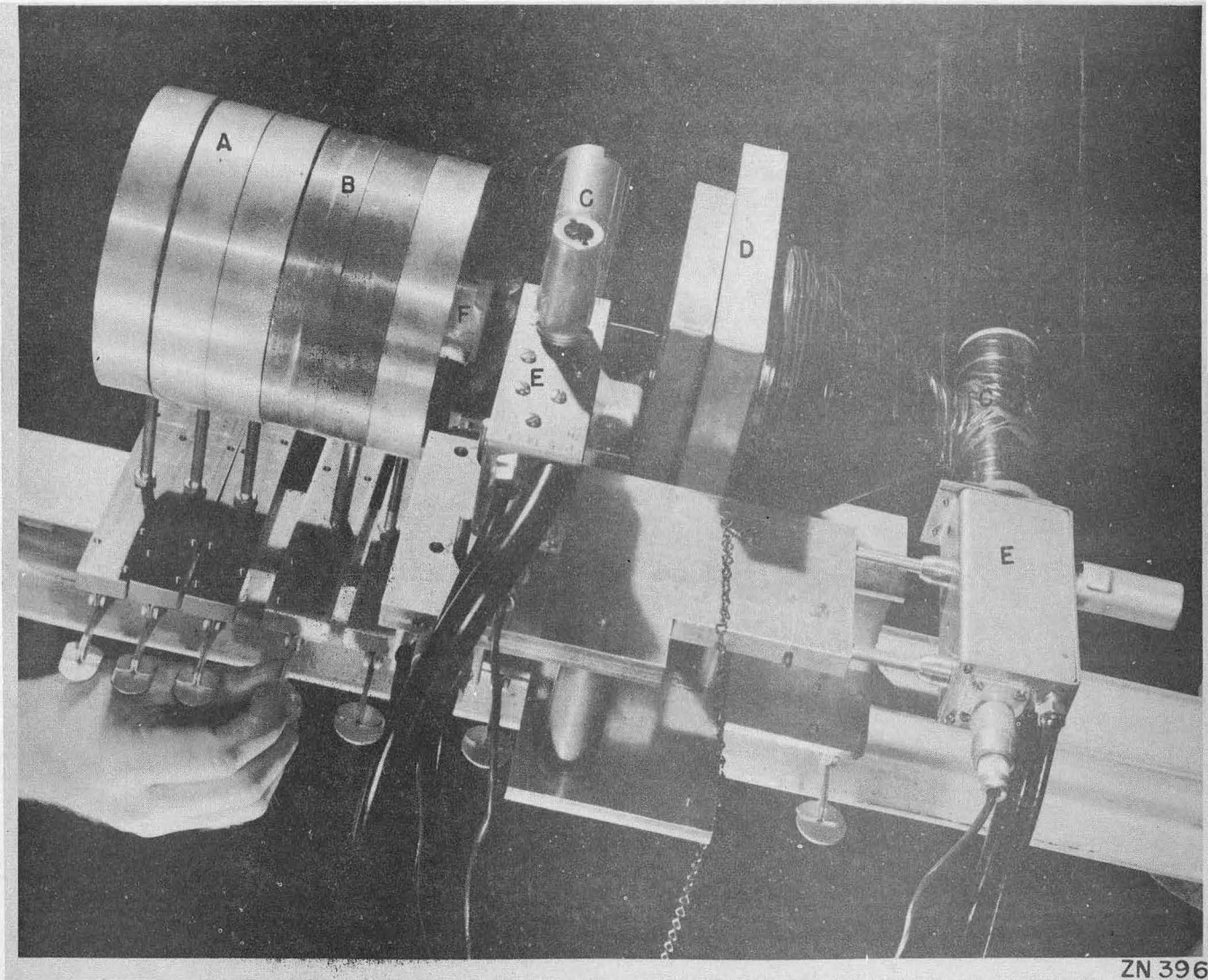
Fig. 3



MU 4081

173 271

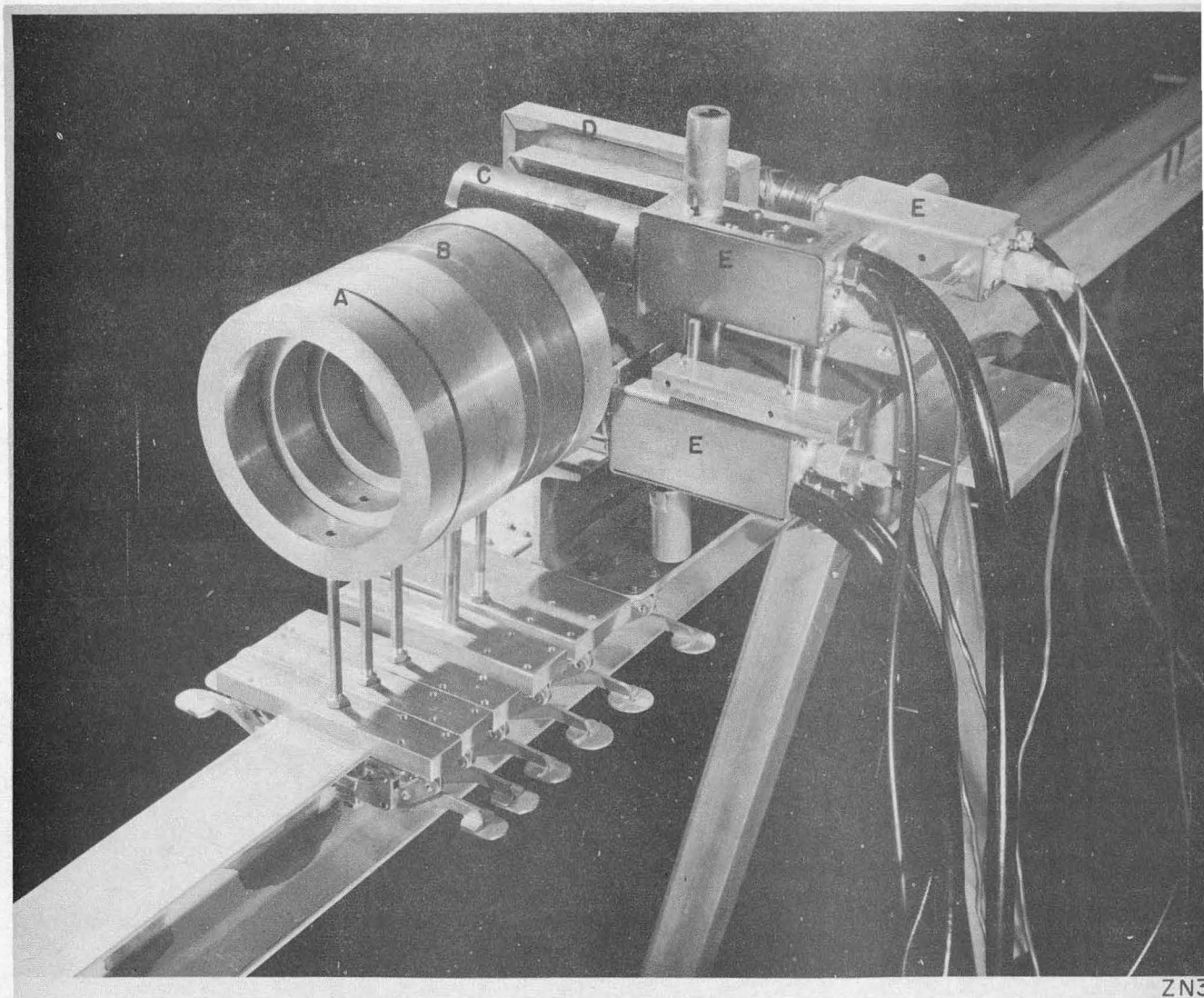
Fig. 4



ZN 396

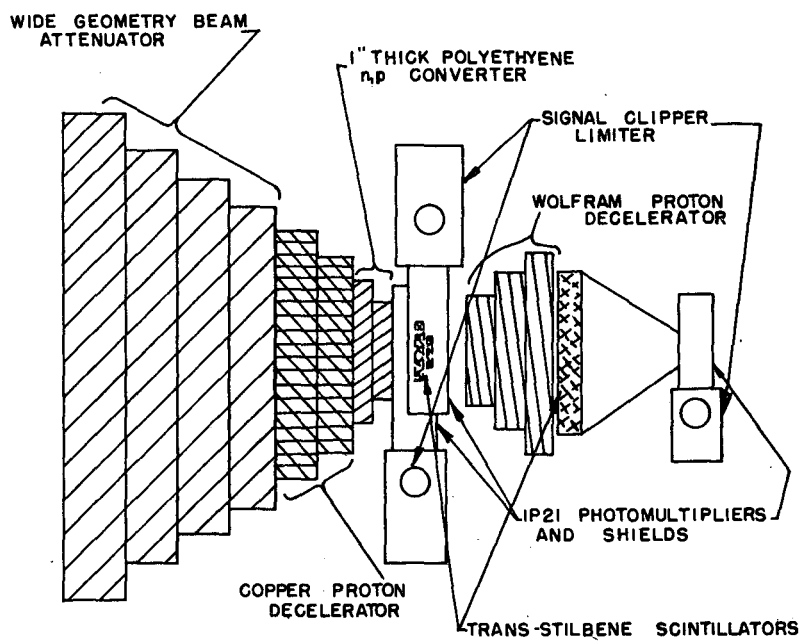
Fig. 5





ZN3

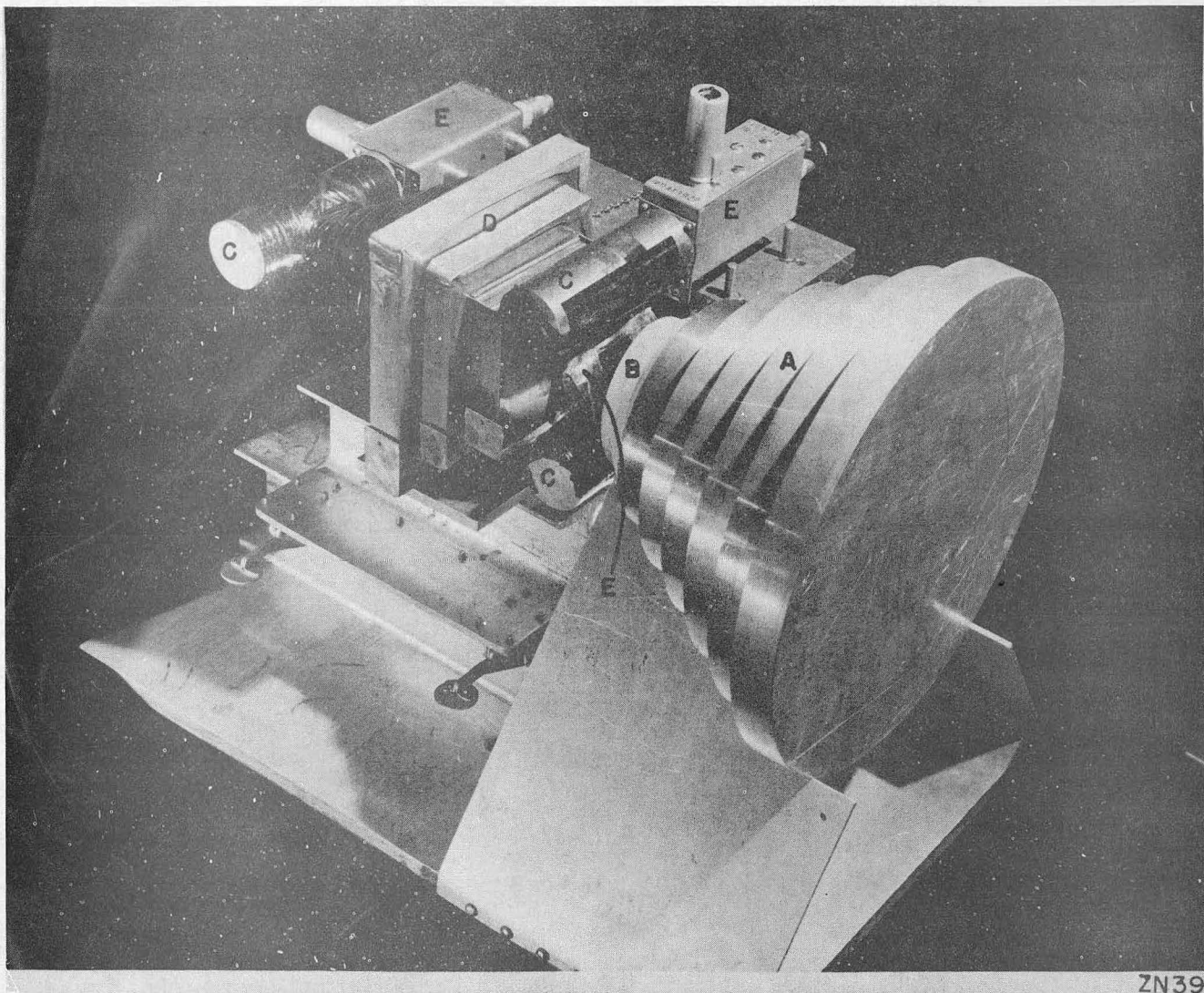
Fig. 6



NEUTRON DETECTOR TELESCOPE (INELASTIC SCATTERING ARRANGEMENT)

MU4080

Fig. 7



ZN399

Fig. 8

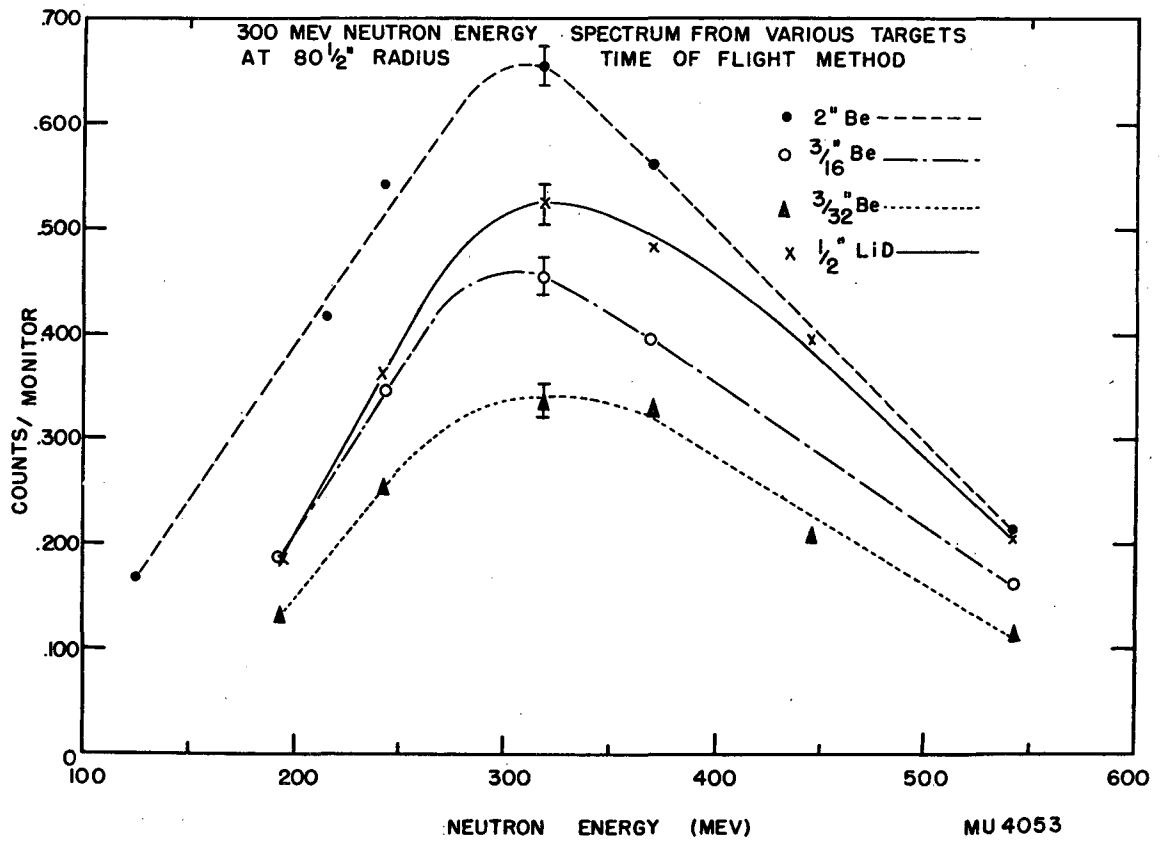


Fig. 9

Donis Munoz  
5545

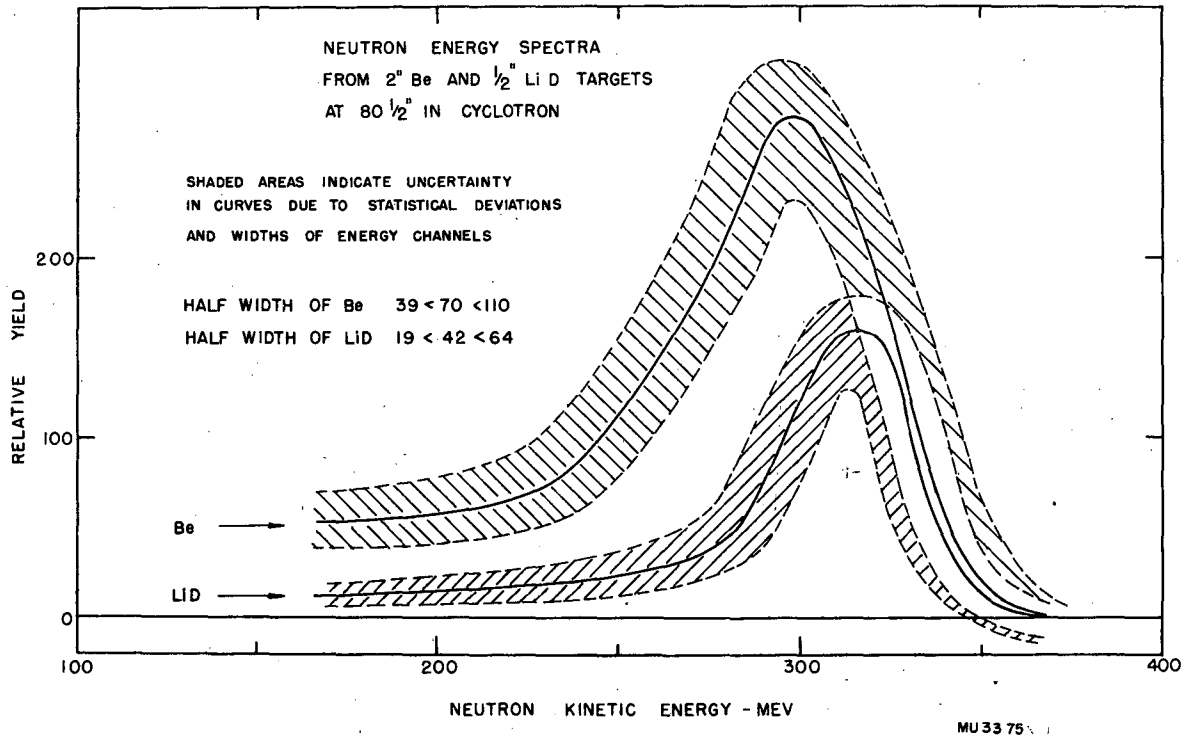


Fig. 10



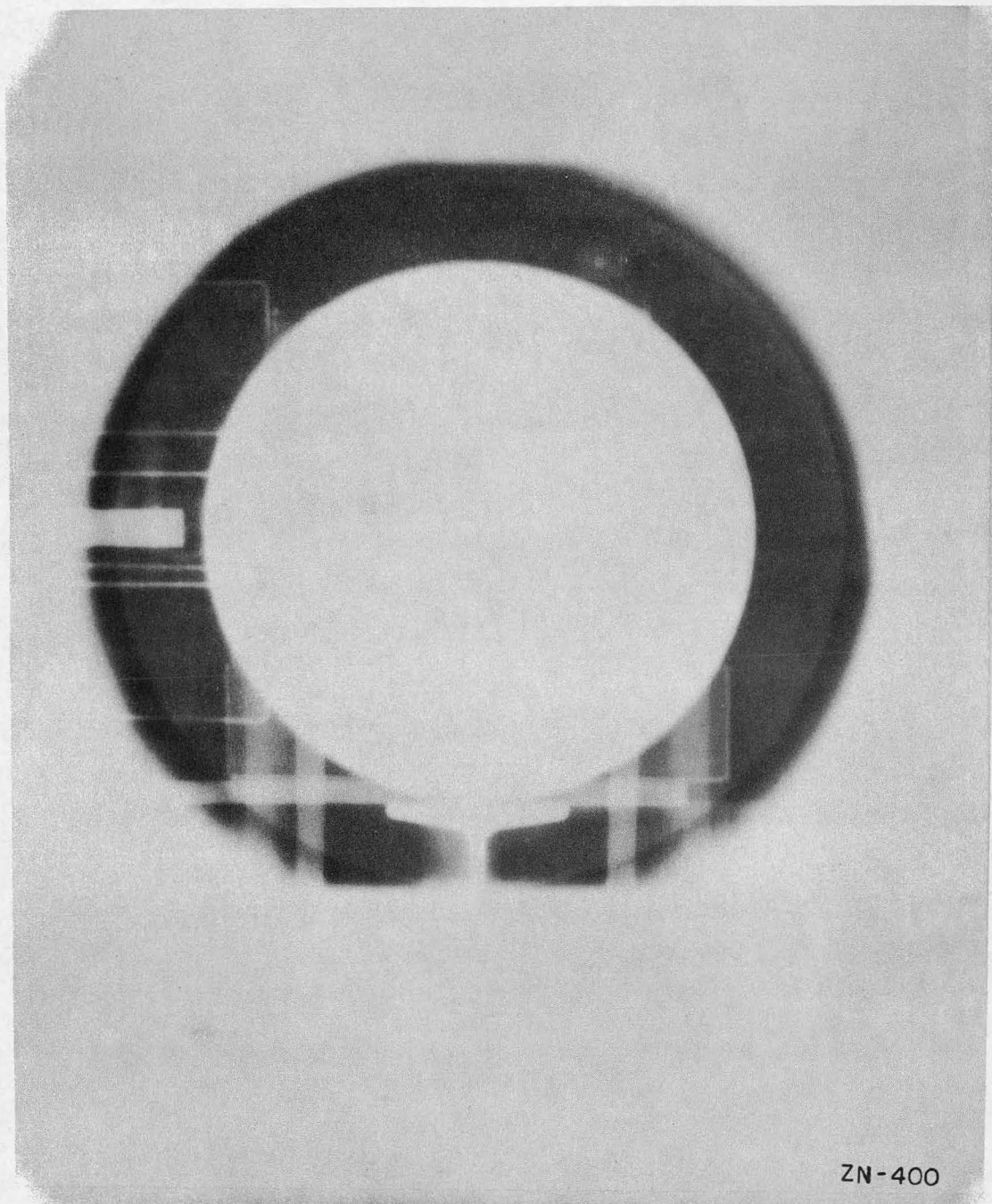
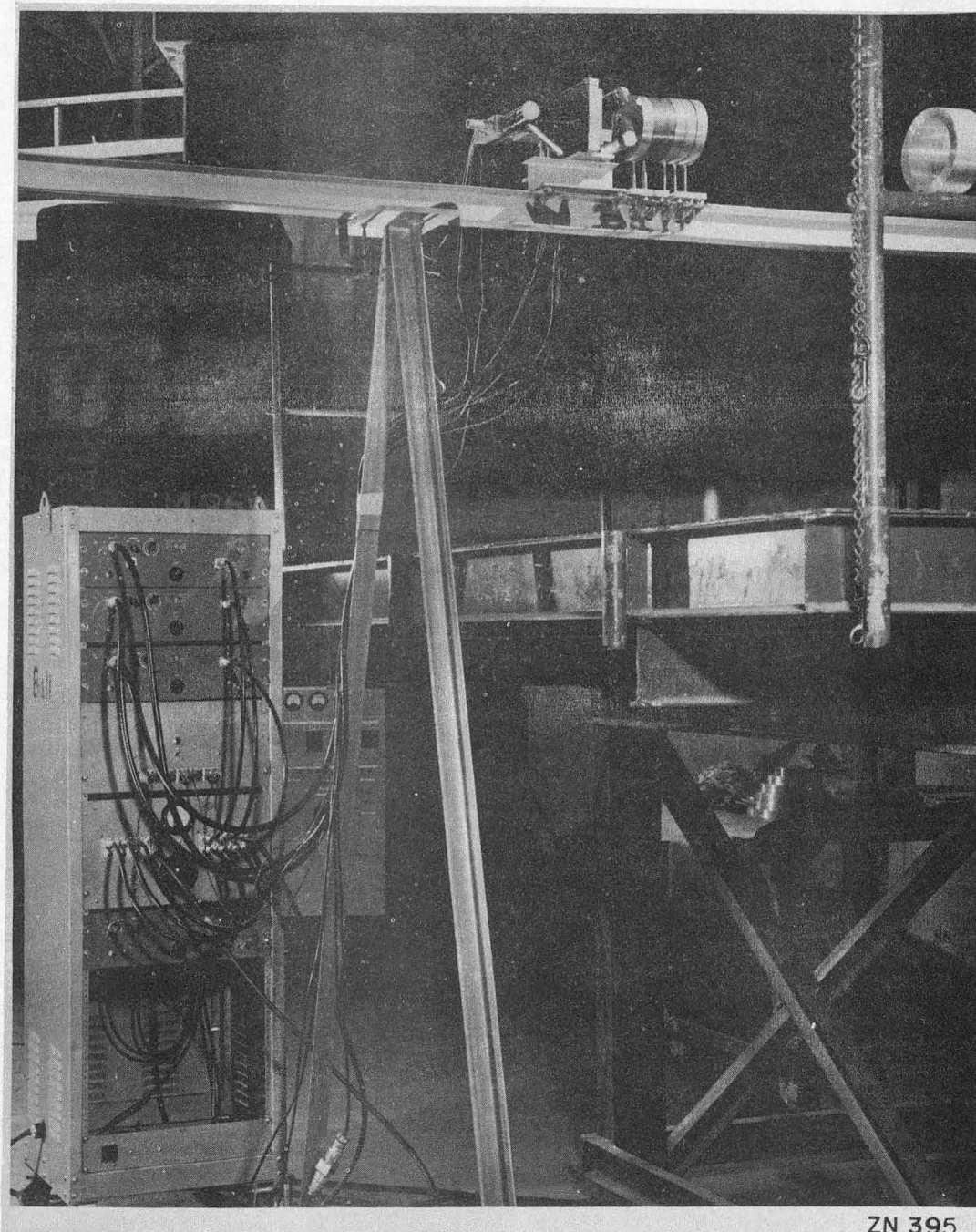


Fig. 11



ZN 395

Fig. 12

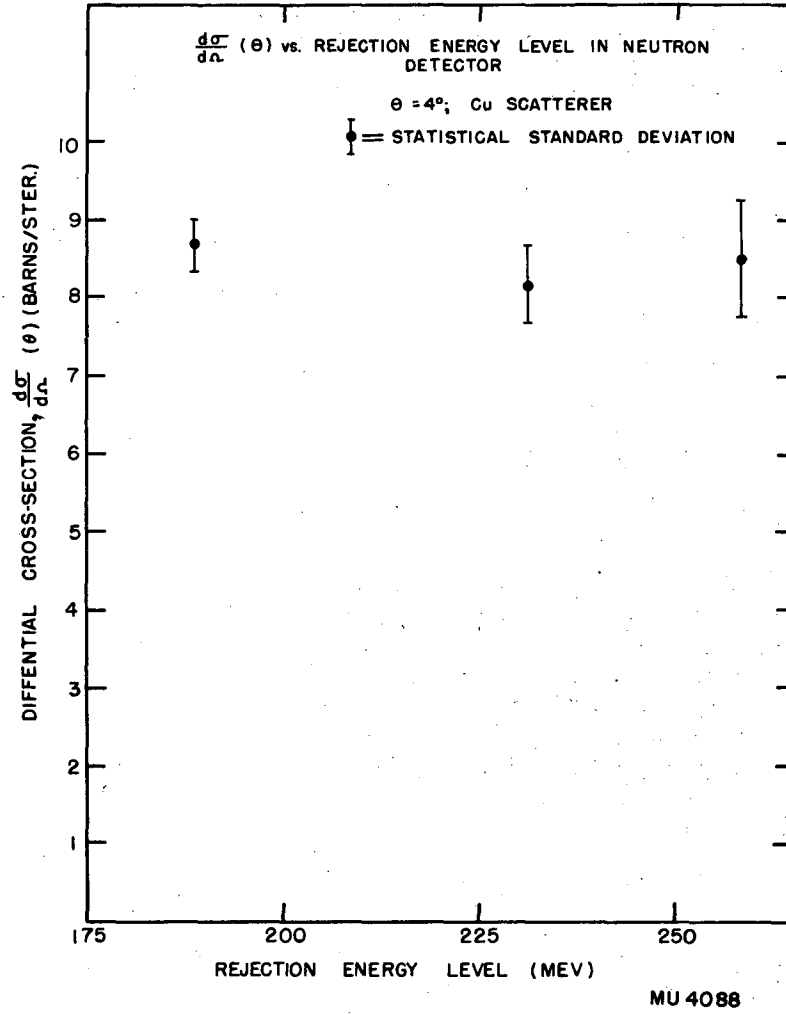
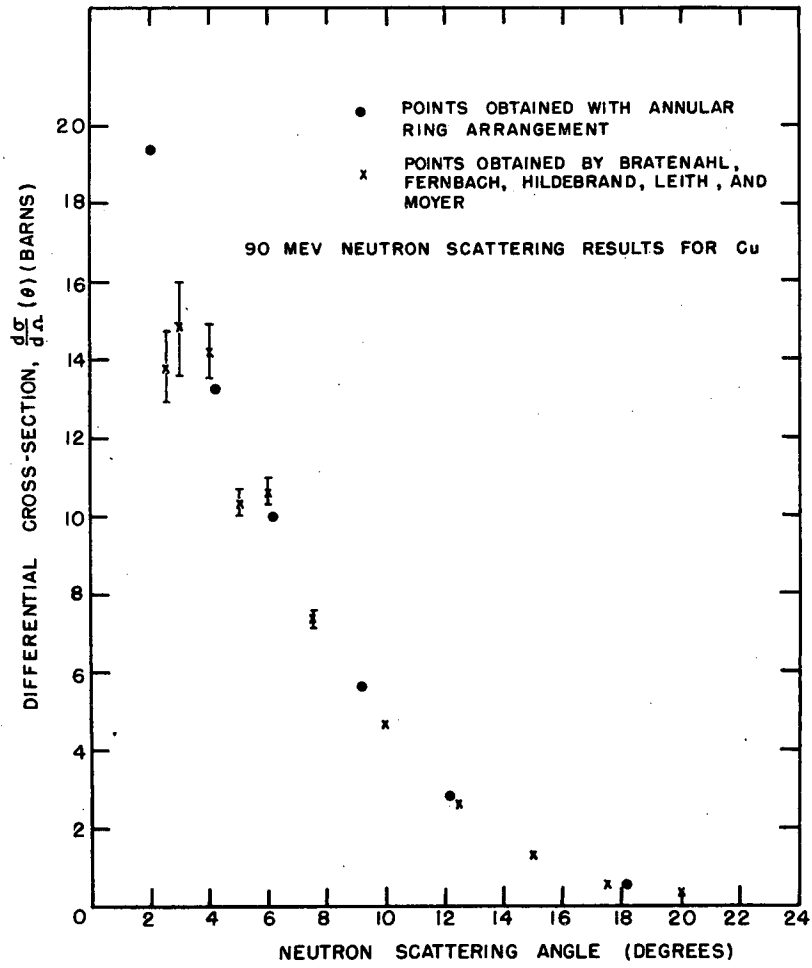


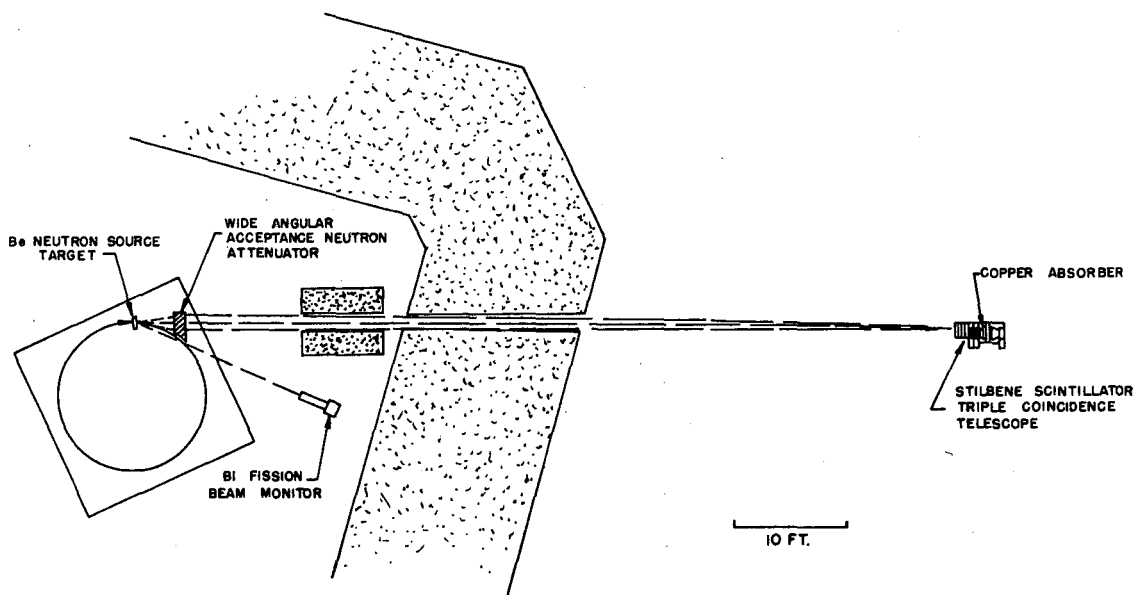
Fig. 13





MU 4086

Fig. 14



ATTENUATOR IN PROXIMITY OF SOURCE ARRANGEMENT

MU4083

Fig. 15

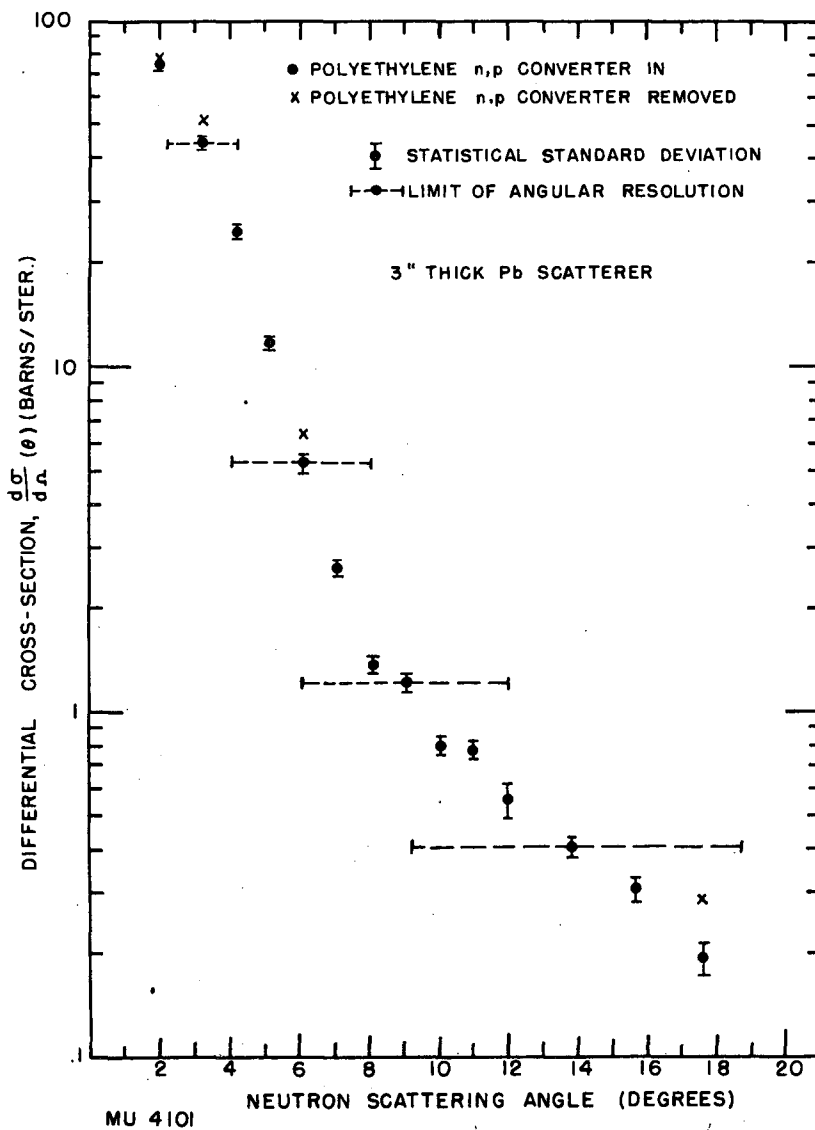


Fig. 16

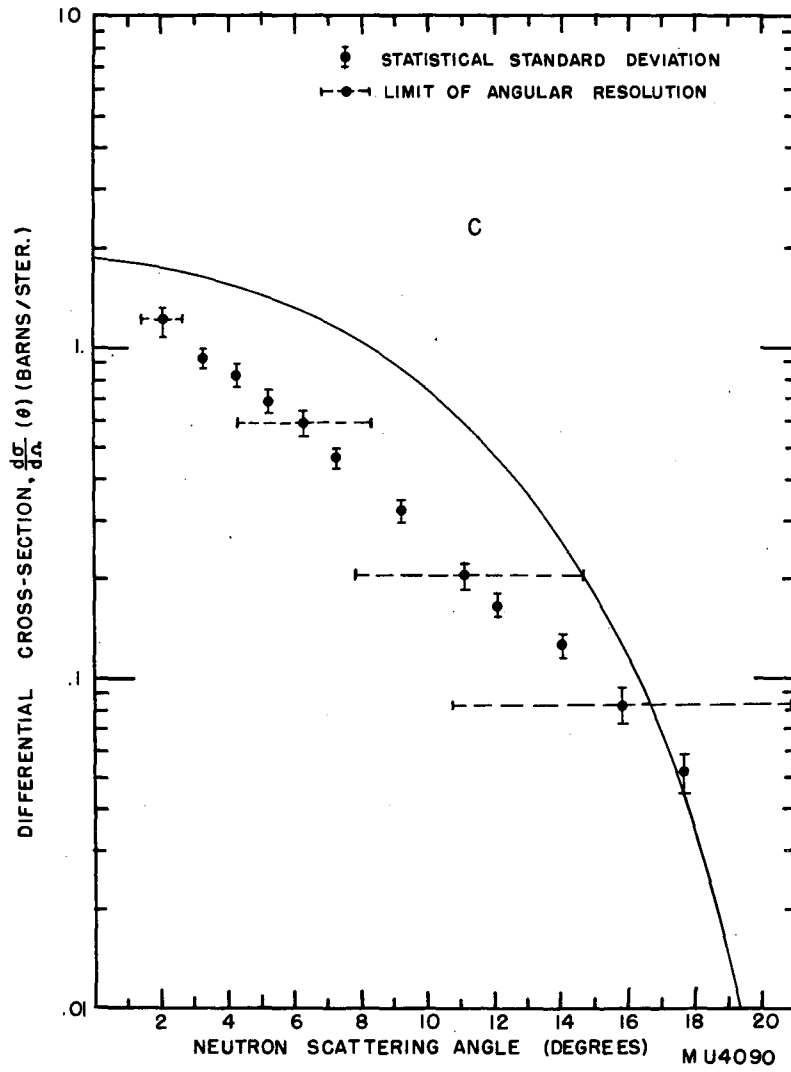


Fig. 17

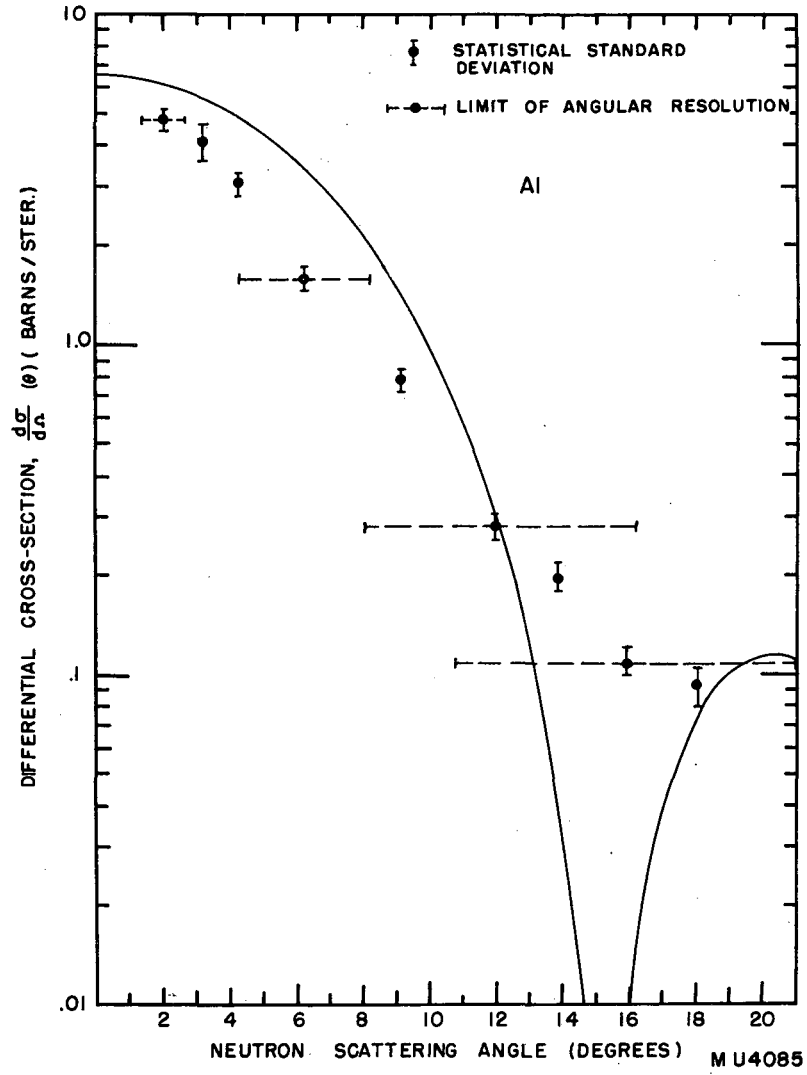


Fig. 18

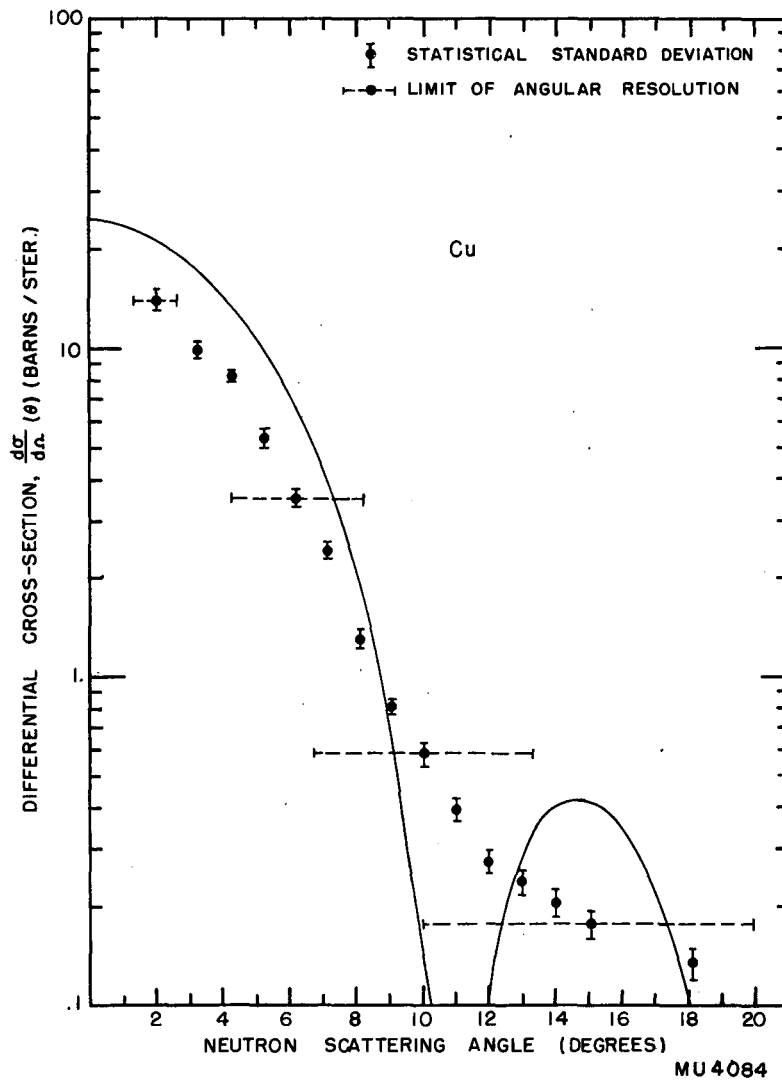


Fig. 19

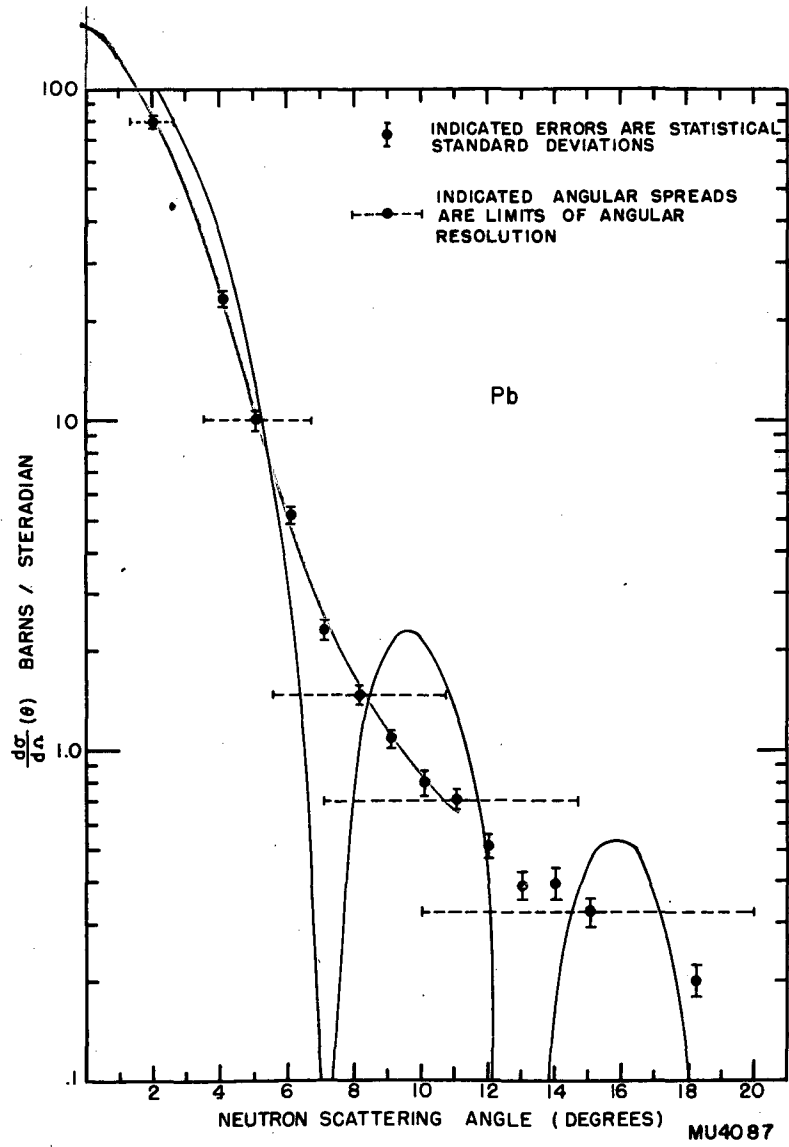


Fig. 20

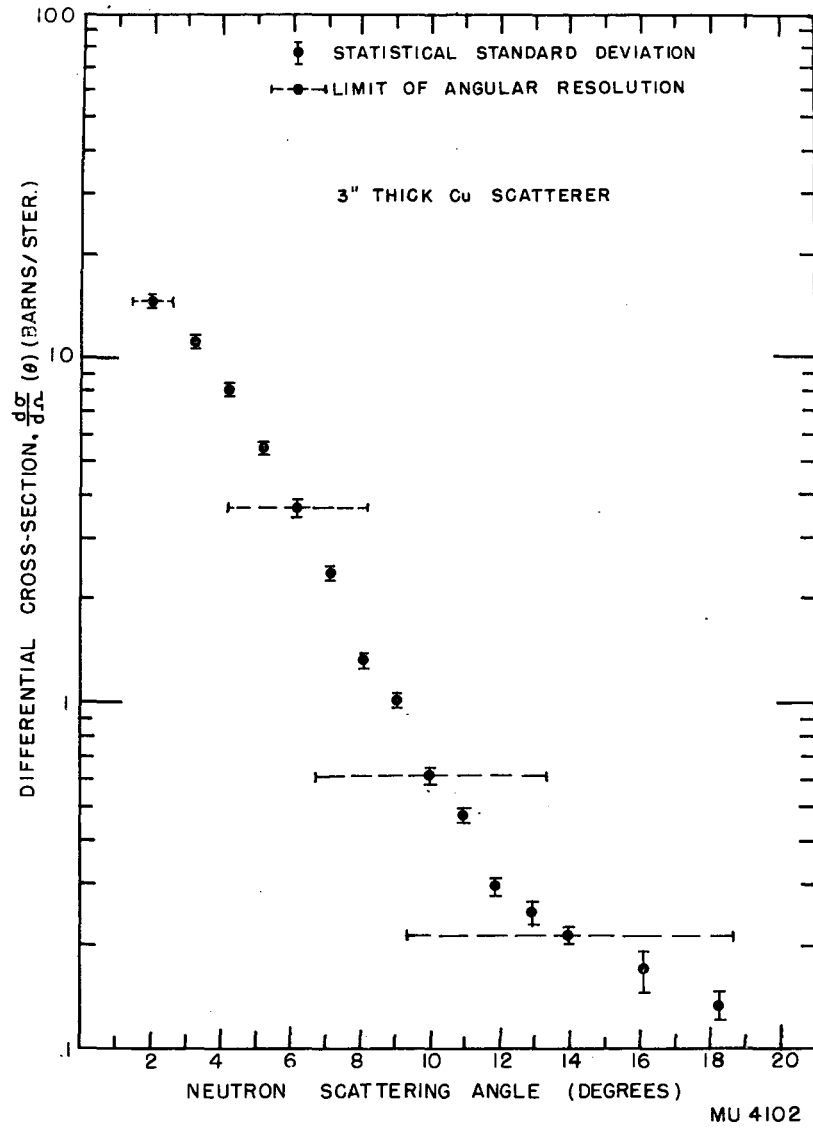
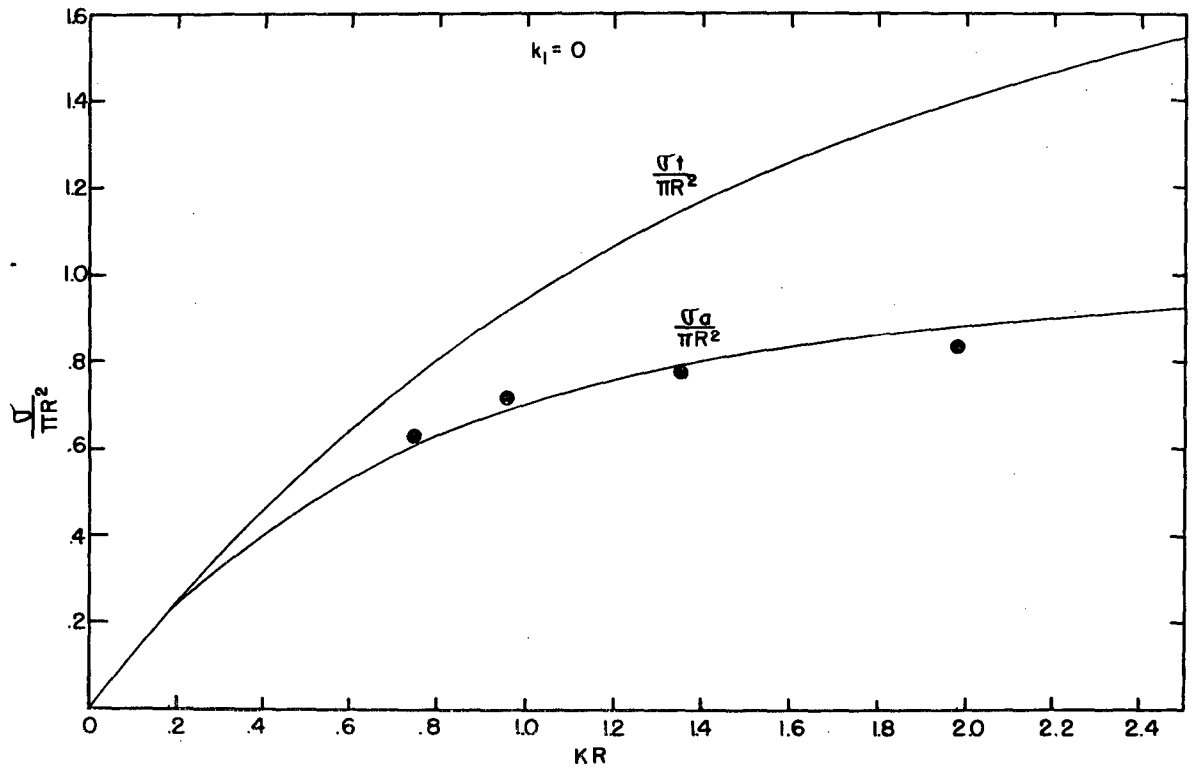


Fig. 21





MU 4079

Fig. 22

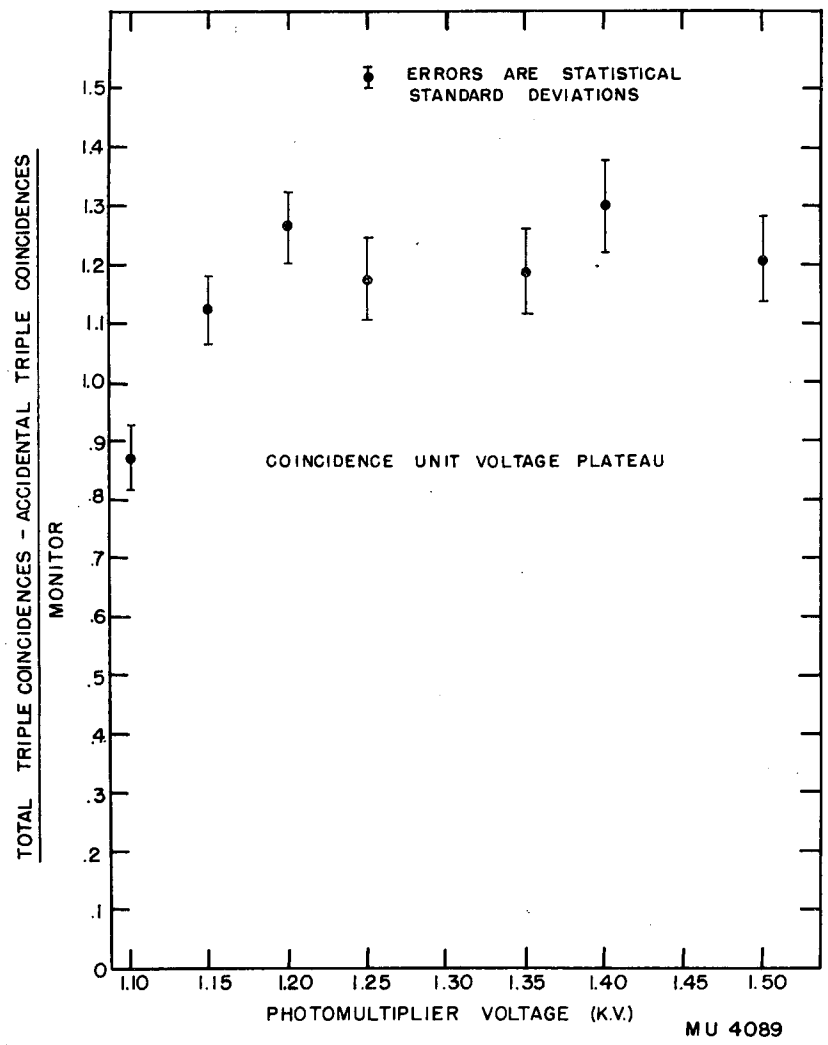


Fig. 23

